Optical Materials 145 (2023) 114393

Contents lists available at ScienceDirect

Optical Materials

journal homepage: www.elsevier.com/locate/optmat

Research Article

An insight into Judd-Ofelt analysis and non-contact optical thermometry of $LiCa_2Mg_2V_3O_{12}$: Dy^{3+} phosphors for multifunctional applications

Raji R [a], Anjana P.S [b], Gopakumar N [a,*]

[a] PG Department of Physics and Research Centre, Mahatma Gandhi College, University of Kerala, Thiruvananthapuram, Kerala, 695004, India

[b] PG Department of Physics, All Saints' College, University of Kerala, Thiruvananthapuram, Kerala, 695007, India

ARTICLE INFO

Keywords:
Cubic garnet
Vanadate
Judd-Ofelt analysis
Optical thermometry

ABSTRACT

A series of Dy^{3+} doped $LiCa_2Mg_2V_3O_{12}$ phosphors have been synthesized by solid state method. The phase composition of the phosphor has been analyzed by X-ray powder diffraction and confirms a cubic phase with Ia-3d space group. The scanning electron microscope images of $LiCa_2Mg_2V_3O_{12}$:xDy^{3+} phosphor reveals the surface morphology and is further investigated by its energy dispersive X-ray spectrum. The elemental mapping analysis displays the uniform composition of the elements present in the phosphor. The band gap energy of the phosphors has been determined from the diffuse reflectance spectra. The Judd-Ofelt intensity parameters are determined from the absorption spectra and follows the trend $\Omega_2 > \Omega_6 > \Omega_4$. The photoluminescence spectra of phosphors excited at 338 nm have intense emission at 494 and 576 nm corresponding to $^4F_{9/2} \rightarrow {}^6H_{15/2}$ and $^4F_{9/2} \rightarrow {}^6H_{13/2}$ transition and is ascribed to the magnetic and electric dipole allowed transition respectively. The radiative parameters for the optimum dopant concentration x = 0.08 has been calculated. Temperature dependent PL spectra of phosphor displays the diverse thermal response of VO_4^{3-} group and Dy^{3+} ion and this can be utilized for the development of thermosensor based on fluorescence intensity ratio (FIR). The phosphor have maximum absolute and relative sensitivity values of 0.0063 K^{-1} and 0.41% K^{-1} in the temperature range of 80–400 K. The optical properties of the phosphor suggest that it find applications in the fields of solid-state lighting, temperature sensing, optoelectronic devices and W-LEDs.

1. Introduction

The investigations on the optical spectra of rare earth ion doped luminescent materials has been an active field of research owing to their wide applications in light emitting diodes, solid-state lasers, electronic products, temperature sensing, optical communications etc. [1,2]. Oxide-based phosphors doped with rare-earth ions exhibit unique electrical and optical properties acquired from the 4f shell of rare-earth ions that aids in modern lighting applications [3]. Moreover, Dy^{3+} doped phosphors gained special attention due to its significance in the production of light emitting materials and visible laser. The luminescence spectrum of Dy^{3+} consists of two prominent emission bands corresponding to the transitions $^4F_{9/2} \rightarrow {}^6H_{15/2}$ (blue) and $^4F_{9/2} \rightarrow {}^6H_{13/2}$ (yellow). An appropriate combination of blue and yellow emission can produce white emission in Dy^{3+} activated phosphors. The transition $^4F_{9/2} \rightarrow {}^6H_{13/2}$ corresponding to the yellow emission is hypersensitive and its intensity of emission strongly depends on the nature of host material. Thus by selecting appropriate host materials, the Dy^{3+} doped phosphors can produce tunable emission [4,5].

The reported inorganic luminescent host materials includes aluminates [6], silicates [7], borates [8], vanadate [9], phosphates [10] etc. Among them self-luminescent vanadate are suitable phosphor host accounting the chemical and thermal stability, facile synthesis methods and low photon energy [11,12]. Furthermore, vanadate phosphors are good host matrix for doping rare earth ions [13]. By incorporating rare earth ions into vanadate matrix, phonon assisted energy transfer from VO_4 to rare earth ions can takes place as well as emissions from both VO_4 and rare earth can occur simultaneously [14]. Based on previous studies it is found that vanadate with cubic garnet structure is gaining much attraction owing to their efficient absorption in the ultraviolet/near-ultraviolet region and have intense emission in the visible region due to the charge transfer transition of $V^{5+} \rightarrow O^{2-}$ in the VO_4 tetrahedron [15]. The garnet phosphors have general stoichiometry $\{A_3\}[B_2]V_3O_{12}$ where, A = Alkaline metals/earth metals, B=Mg, Zn, Sc, Y and lanthanides [11]. The flexibility of ionic substitution in the crystal structure leads to various chemical composition [14].

* Corresponding author.
E-mail address: gopkumar.n@gmail.com (G. N).

https://doi.org/10.1016/j.optmat.2023.114393
Received 13 July 2023; Received in revised form 5 September 2023; Accepted 19 September 2023

From literature point of view, the luminescence emission of rare earth free $LiCa_3MV_3O_{12}$ (M = Zn, Mg) [16] phosphor have bluish-white emission whereas rare earth activated cubic garnet phosphors $Ca_3LiMgV_3O_{12}$:Eu^{3+} [14,17], $LiCa_3MgV_3O_{12}$:Sm^{3+} [18], $Ca_3LiZnV_3O_{12}$:Eu^{3+} [11] has tunable emission. The vanadate garnet phosphors $Ca_2NaMg_2V_3O_{12}$:Eu^{3+} [19,20], $Ca_2NaMg_2V_3O_{12}$:Dy^{3+},$Sm3^{+}$ [21,22], $Ca_2KZn_2V_3O_{12}$ [23,24], $Ca_2KMg_2V_3O_{12}$:Dy^{3+} [25] are reported to emit white color. The other cubic garnet systems such as $Na_2YMg_2V_3O_{12}$:Eu^{3+} [26], $Na_2YMg_2V_3O_{12}$:Er^{3+},Yb^{3+} [27], $LiCa_2Mg_2V_3O_{12}$:Eu^{3+} [28], $LiCa_2SrMgV_3O_{12}$:Eu^{3+} [13] are capable to produce tunable emission. The estimation of Judd-Ofelt intensity parameters using absorption spectra is a less explored territory [29]. To best of our knowledge, the absorption spectra analysis using Judd-Ofelt theory and thermometry properties of $LiCa_2Mg_2V_3O_{12}$:Dy^{3+} phosphors are not reported yet. The optical thermometry based on fluorescence intensity ratio (FIR) have advantages over other methods due to its fast response, high resolution and non-contact measurement in harsh environments. In RE-activated vanadate garnet system, the FIR between VO_4^{3-} group and RE ion is used for the thermo-sensor activity studies [2]. Moreover, thermometry measurements on Dy^{3+} activated vanadate garnets are rare and the research that promotes development of such materials need more attention.

In this present work, Dy^{3+} doped $LiCa_2Mg_2V_3O_{12}$ phosphor is prepared via solid state reaction method in air atmosphere. The structural, morphological, optical, luminescence and thermometry properties of the prepared phosphors have been discussed in detail. The Judd-Ofelt intensity parameters (Ω_2, Ω_4, Ω_6) of $LiCa_2Mg_2V_3O_{12}$:$0.08Dy^{3+}$ phosphor are evaluated from the absorption spectra for the first time. The energy transfer between VO_4 and Dy^{3+}, chromaticity coordinates and quantum efficiency are also investigated.

2. Experimental section

2.1. Materials and synthesis

$LiCa_2Mg_2V_3O_{12}$:xDy^{3+} (x = 0, 0.005, 0.0075, 0.02, 0.04, 0.06, 0.08, 0.1) phosphors were perpared by conventional solid-state reaction method. Stochiometric ratio of high purity oxides $CaCO_3$ (Sigma Aldrich), Li_2CO_3 (Sigma Aldrich),V_2O_5 (Sigma Aldrich), $(MgCO_3)_4 \bullet Mg(OH)_2 \bullet 5H_2O$ (Sigma Aldrich) and Dy_2O_3 (Sigma Aldrich) were weighed and well mixed in an agate mortar for 1 h. The mixtures were dried and ground before the calcination process. The powders were calcined at 800 °*C* for 3 h in a muffle furnace. The obtained final products were crushed and reground for characterizations.

2.2. Characterization

The phase purity and crystalline nature of phosphors were examined by powder X-ray diffractometer (D8 Advanced Bruker) with Ni-filtered Cu-Kα (λ = 1.5406Å). The morphology of the synthesized samples was recorded using scanning electron microscope (Nova Nano SEM 450, FEI-Nova Model No.1027647), with an acceleration voltage of 15 kV, equipped with XFlash detector 6/10 (Bruker). The energy dispersive X-ray spectrometer (Carl Zeiss EVO 18 Research) was used to carry out elemental analysis of the phosphor. The optical band gap energy of phosphors were determined based on diffuse reflectance spectra, monitored using JASCO V-550 UV–Vis double beam spectrophotometer with integrating sphere (ISV-469) attachment. The room temperature UV–Vis–NIR absorption spectra of $LiCa_2Mg_2V_3O_{12}$:0.08 Dy^{3+} phosphor was measured using Agilent Cary-5000 UV–Vis–NIR spectrophotometer with integrating sphere attachment. The photoluminescence, PLE Spectra and luminescence decay lifetime of the phosphors were measured using Horiba Jobin Yvon Flourolog III. The Quantum yield and temperature dependent PL of the phosphor were measured by EDINBURGH FLS 1000 Fluorescence Spectrometer. The sample code for the prepared phosphors was taken as LCMV, LCMV:0.005Dy^{3+},LCMV:0.0075Dy^{3+}, LCMV:0.02Dy^{3+}, LCMV:0.04Dy^{3+}, LCMV:0.06Dy^{3+}, LCMV:0.08Dy^{3+} and LCMV:0.1Dy^{3+} for $LiCa_2Mg_2V_3O_{12}$ with x = 0, 0.005, 0.0075, 0.02, 0.04, 0.06, 0.08 and 0.1 respectively.

3. Results and discussion

3.1. Structural and morphological properties

3.1.1. X-ray diffraction

The XRD pattern of $LiCa_2Mg_2V_3O_{12}$:xDy^{3+} (x = 0, 0.005, 0.0075, 0.02, 0.04, 0.08, 0.1) phosphors are shown in Fig. 1. All the peak positions of $LiCa_2Mg_2V_3O_{12}$:xDy^{3+} samples well match to the standard ICDD card no. 00-024-1212. The $LiCa_2Mg_2V_3O_{12}$ exhibits a cubic crystal structure with Ia-3d (230) space group. The crystal structure of LCMV consists CaO_8 dodecahedron, MgO_6 octahedron and VO_4 tetrahedron. The Ca^{2+} ions and one Mg^{2+} are coordinated to eight O ions and the centre of octahedron is constituted by Mg^{2+} and Li^{+} ions. The V^{5+} ions and four O^{2-} ions occupies the VO_4 tetrahedron [16]. The lattice parameters are a = b = c = 12.3967 Å, V = 1905.1096 $Å^3$, α = β = γ = 90 ° and Z = 8. When Dy^{3+} ions are incorporated into the system in smaller amounts no impurity phases are detected. When dopant concentrarion exceeds 2 mol %, impurity peaks appear due to solubility limitation of Dy^{3+} ions in vanadate garnet [14]. The trace of impurity corresponds to the $DyVO_4$ (ICDD card no. 00-016-0870) phase and is consistent with that of the previously reported works [30].

The substituition relation of Dy^{3+} in $LiCa_2Mg_2V_3O_{12}$ host is evaluated by the radius difference percentage (D_r) formula given by Pires and Davolos [21]. According to this, the precentage difference of radius (D_r) between the activator and replaced ion should be less than 30%. The D_r value is calculated using the following expression:

$$D_r = 100\% \times \frac{R_{m(C.N)} - R_{d(C.N)}}{R_{m(C.N)}} \quad (1)$$

where C.N is the coordination number, $R_{m(C.N)}$ is the ionic radii of replaced cation and $R_{d(C.N)}$ is the ionic radii of activator ion. The D_r values of Dy^{3+} (1.02 Å, C.N = 8) and Ca^{2+} (1.12 Å, C.N = 8), Li^{+} (0.76 Å, C.N = 6), Mg^{2+} (0.72 Å, C.N = 6), V^{5-} (0.355 Å, C.N = 4) are 8.92%, −34.21%, −41.66%, −187.32% respectively [15,30–32]. In $LiCa_2Mg_2V_3O_{12}$:xDy^{3+} phosphor, Dy^{3+} replaces Ca^{2+} as the D_r value is 8.92%.

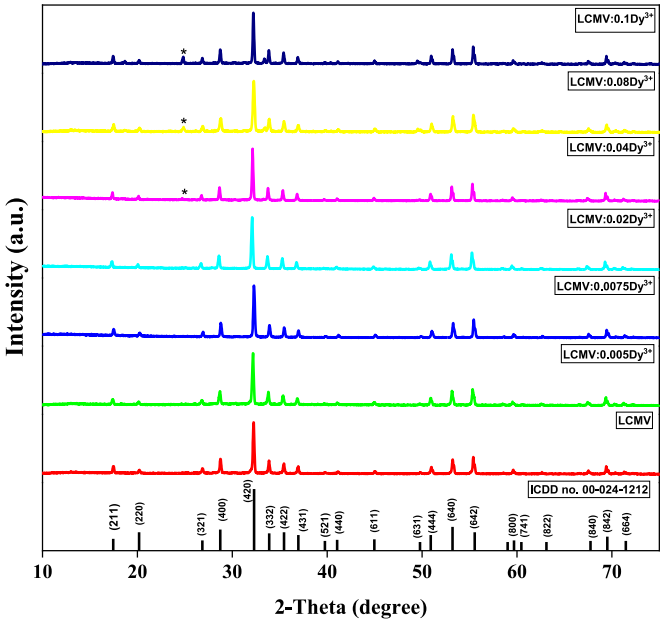

Fig. 1. XRD patterns of ICDD card no. 00-024-1212 and $LiCa_2Mg_2V_3O_{12}$:xDy^{3+} (x = 0, 0.005, 0.0075, 0.02, 0.04, 0.08, 0.1).

3.1.2. FESEM analysis

The FESEM analysis of $LiCa_2Mg_2V_3O_{12}$:xDy^{3+} (x = 0, 0.06, 0.08, 0.1) phosphors are shown in Fig. 2 (a-d). All the samples show similar morpholgy with irregular shape. The average grain size of phosphors varies between 6 and 9 μm. The grain size of phosphors increases with increase in dopant cocentartion.

3.1.3. EDX and elemental mapping

The EDX spectra of $LiCa_2Mg_2V_3O_{12}$ and $LiCa_2Mg_2V_3O_{12}$:$0.08Dy^{3+}$ phosphors are displayed in Fig. 3 (a-b). The EDX spectra depicts the characteristic energy peaks of Ca, Mg, V, O for the undoped sample and for the doped sample Ca, Mg, V, O and Dy peaks. Li is undetectable in EDX spectra as it have lighter molar mass [16]. The atomic percentage of samples are also shown in Table 1. The measured EDX result confirms the elemental composition of synthesized phosphors. Fig. 4 (a-b) shows the elemental mapping of $LiCa_2Mg_2V_3O_{12}$ and $LiCa_2Mg_2V_3O_{12}$:$0.08Dy^{3+}$ phosphors respectively. The elemental mapping shows that distribution of Ca, Mg, V and O are homogenous in undoped $LiCa_2Mg_2V_3O_{12}$ system. The Dy^{3+} doped $LiCa_2Mg_2V_3O_{12}$ phosphor also exhibits similar distribution as that of $LiCa_2Mg_2V_3O_{12}$ which confirms the effective incorporation of dysprosium ion into host lattice.

3.2. Optical properties

3.2.1. Absorption spectra

The optical absorption spectrum of $LiCa_2Mg_2V_3O_{12}$:$0.08Dy^{3+}$ phosphor in UV–Vis–NIR region is shown in Fig. 5. The absorption spectrum in UV region consists of CT band of $LiCa_2Mg_2V_3O_{12}$ and NIR region consists of characteristic absorption bands of Dy^{3+} originated from $^6H_{15/2}$ ground state to other excited states. The NIR region has six sharp bands corresponding to the induced electric dipole transitions in Dy^{3+}. The absorption peaks at 5952, 7680, 9033, 11013, 12360 and 13192 cm^{-1} are ascribed to the transitions from ground level $^6H_{15/2}$ to $^6H_{11/2}$,$^6F_{11/2}$,$^6F_{9/2}$,$^6F_{7/2}$,$^6F_{5/2}$ and $^6F_{3/2}$ respectively. The band position and intensities of some rare earth ions are hypersensitive to the local ligand field of the ion. In the case of Dy^{3+} the intensity of hypersensitive transition $^6H_{15/2} \rightarrow {}^6H_{11/2}$ is found to be more intense [33].

The bonding nature of Dy^{3+} in $LiCa_2Mg_2V_3O_{12}$ host can be inferred by calculating the nephelauxetic ratio (β) and the bonding parameter (δ). The nephelauxetic ratio can be calculated by the equation [34]:

$$\beta = \frac{\nu_c}{\nu_a} \tag{4}$$

where ν_c is the peak positions in cm^{-1} corresponding to the transitions of $LiCa_2Mg_2V_3O_{12}$:$0.08Dy^{3+}$ and ν_a corresponds to the transitions of aqueous solution in cm^{-1}. The bonding parameter is determined using the equation:

$$\delta = \frac{1-\overline{\beta}}{\overline{\beta}} \times 100 \tag{5}$$

where $\overline{\beta}$ corresponds to the average nephelauxetic ratio for all the absorption transitions present in the absorption spectra. Based on bonding parameter value the nature of interaction of Dy^{3+} ion with surroundings can be covalent or ionic. A positive sign implies covalent nature whereas negative to the ionic nature [35].

The determined values of the nephelauxetic ratio (β) and the bonding parameter (δ) are presented in Table 2. The average value of β ($\overline{\beta}$) is 0.9999 and the bonding parameter (δ) is calculated to be 0.0100. The positive value of δ indicates the covalent nature of Dy^{3+} ion in $LiCa_2Mg_2V_3O_{12}$ host.

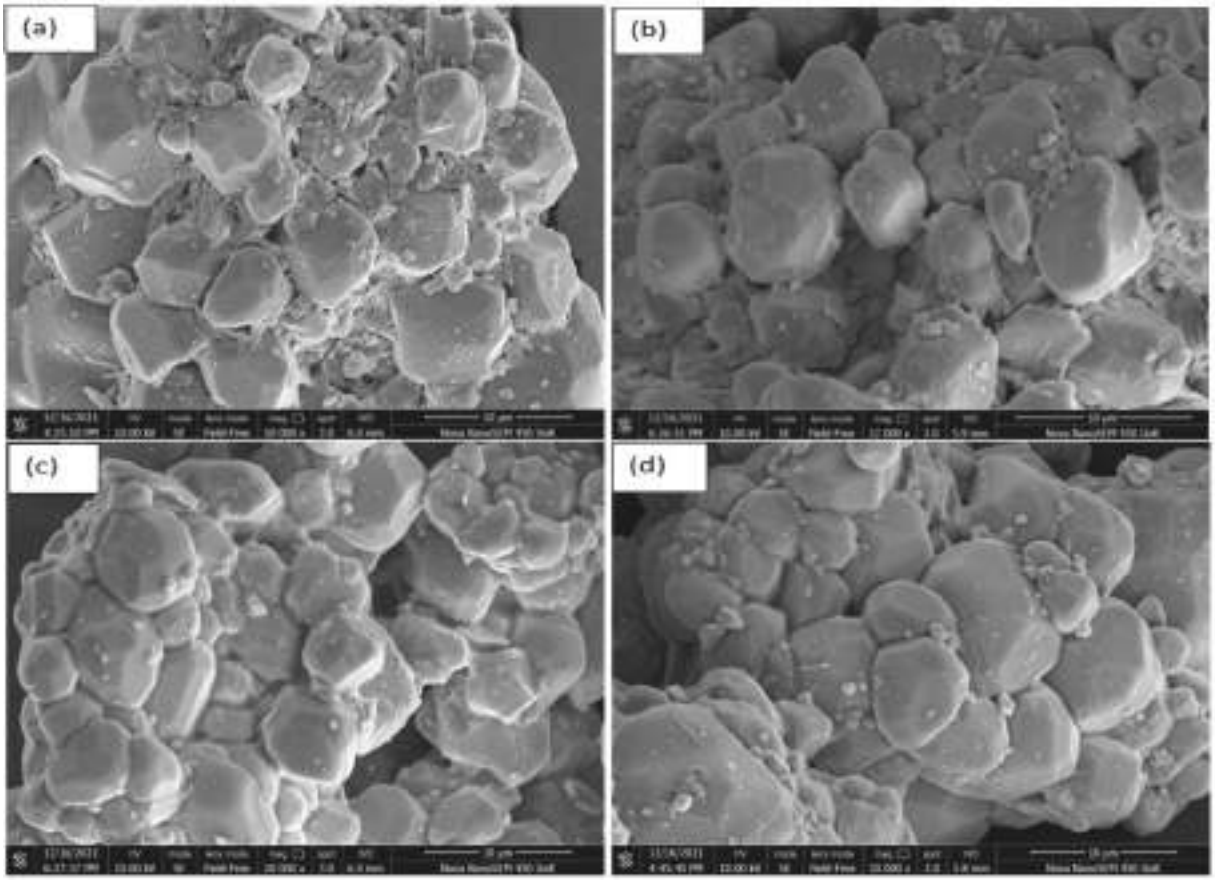

Fig. 2. The FESEM analysis of $LiCa_2Mg_2V_3O_{12}$:xDy^{3+} **(a)** x = 0, **(b)** x = 0.06, **(c)** x = 0.08, **(d)** x = 0.1 phosphor.

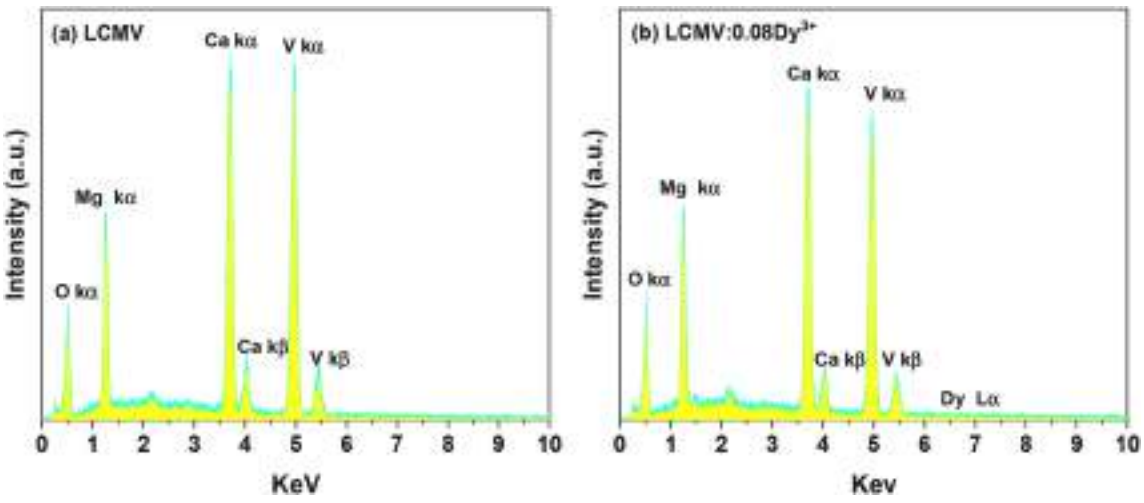

Fig. 3. (a) EDX Spectra of $LiCa_2Mg_2V_3O_{12}$ phosphor **(b)** EDX Spectra of $LiCa_2Mg_2V_3O_{12}$:0.08Dy^{3+} phosphor.

Table 1
EDX spectra analysis of $LiCa_2Mg_2V_3O_{12}$ and $LiCa_2Mg_2V_3O_{12}$:0.08Dy^{3+} phosphors.

Element	Energy (KeV)	Atomic %	
		$LiCa_2Mg_2V_3O_{12}$	$LiCa_2Mg_2V_3O_{12}$:0.08Dy^{3+}
Ca	3.69	17.37	16.83
Mg	1.24	14.99	13.56
V	4.95	22.65	21.13
O	0.52	45.00	48.03
Dy	6.49	–	0.51

3.2.2. Diffuse reflectance spectra

In order to decipher the influence of dopant concentration on bandgap energy the diffuse reflectance spectra of phosphors are monitored and the Tauc analysis is performed. The diffuse reflectance spectra of $LiCa_2Mg_2V_3O_{12}$:xDy^{3+} (x = 0.005, 0.0075, 0.02, 0.04, 0.08, 0.1) phosphors are shown in Fig. 6.

The band gap value is determined using the relation:

$$(\alpha h\nu)^n = A(h\,\nu - E_g) \tag{6}$$

where hν-photon energy, α-absorption coefficient and A-absorption constant. For direct transition the n value is chosen as 2. The absorption coefficient α is calculated from the observed reflectance of phosphors using the formula [14]:

$$\alpha = \frac{(1-R)^2}{2R} \tag{7}$$

From the Tauc plot as shown in Fig. 7, the band gap values of $LiCa_2Mg_2V_3O_{12}$:xDy^{3+} (x = 0, 0.005, 0.0075, 0.02, 0.04, 0.08, 0.1) phoshors are found out to be 3.36, 3.40, 3.41, 3.37, 3.40, 3.42 and 3.43 eV respectively. In the case of undoped phosphor the band gap energy is the energy difference between the edges of valence band and conduction band. The band gap energy broadened with doping, this can be elucidated by Burstein Moss effect. The dopant donor electrons occupies the lower level of conduction band which shifts the Fermi levels towards the conduction band. The lower levels of conduction band is blocked due to the partial filling and as a result of this band gap value broadens. The energy of exciting photon (338 nm) is 3.66 eV and is higher than the band gap value of all the $LiCa_2Mg_2V_3O_{12}$:xDy^{3+} phosphors. Thus the excitation efficiently give rise to intense emission [35]. The refractive index of the $LiCa_2Mg_2V_3O_{12}$:x Dy^{3+} phosphor can be calculated by Dimithrov-Sakka relation using the band gap value. The relation is as follows [36]:

$$\frac{(n^2-1)}{(n^2+2)} = 1 - \sqrt{\frac{E_g}{20}} \tag{8}$$

where n is the refractive index and E_g represents the band gap energy of the system. The refractive index of $LiCa_2Mg_2V_3O_{12}$:0.08Dy^{3+} phosphor is found to be 2.30 and can be used for the further calculations of Judd-Ofelt analysis.

3.2.3. Judd-Ofelt analysis

Judd-Ofelt analysis provides more information about the chemical interaction and local structure between rare earth ions and ligand field [37–39]. The calculated and measured line strengths of absorption bands of Dy^{3+} doped $LiCa_2Mg_2V_3O_{12}$ are determined using the following relations [40]:

$$S_{cal} = \sum_{\lambda=2,4,6} \Omega_\lambda \left|\langle (S,L)J \| U^{(\lambda)} \| (S',L')J' \rangle\right|^2 \tag{9}$$

Where Ω_λ are the Judd-Ofelt (J-O) intensity parameters ($\Omega_2, \Omega_4, \Omega_6$) and $\langle \| U^\lambda \| \rangle$ is the doubly reduced matrix elements of the unit tensor operator of rank λ which are calculated using intermediate coupling approximation.

$$S_{meas} = \frac{3hc(2J+1)}{8\pi^3 e^2 \bar{\lambda}}\, n \left(\frac{3}{n^2+2}\right)^2 \int \sigma(\lambda) d\lambda \tag{10}$$

where $\bar{\lambda}$ is mean wavelength corresponds to the particular absorption transition of a band, J is the total angular momentum quantum number of initial state, n is the refractive index of host

and $\int \sigma(\lambda) d\lambda$ is integrated absorption cross section. The absorption cross-section $\sigma(\lambda)$ is determined using the relation:

$$\sigma(\lambda) = \frac{2.303 * A}{tN} \tag{11}$$

where A is the absorbance, t = 0.1 cm is the thickness of sample and N is the Dy^{3+} ion concentration/cm^3 [29,41]. The integrated absorption cross section $\int \sigma(\lambda) d\lambda$ for each band of absorption is evaluated from Fig. 8.The Judd-Ofelt intensity parameters are obtained by least squares fit method to the calculated and measured line strengths [40]. The J-O parameters (Ω_2, Ω_4, Ω_6) and line strengths are presented in Table 3. From the table it is evident that J-O parameter follows the trend $\Omega_2 > \Omega_6 > \Omega_4$, which indicates the covalency between Dy^{3+} ion and host matrix. The J-O parameter Ω_2 elucidate the covalency of bond whereas Ω_4 and

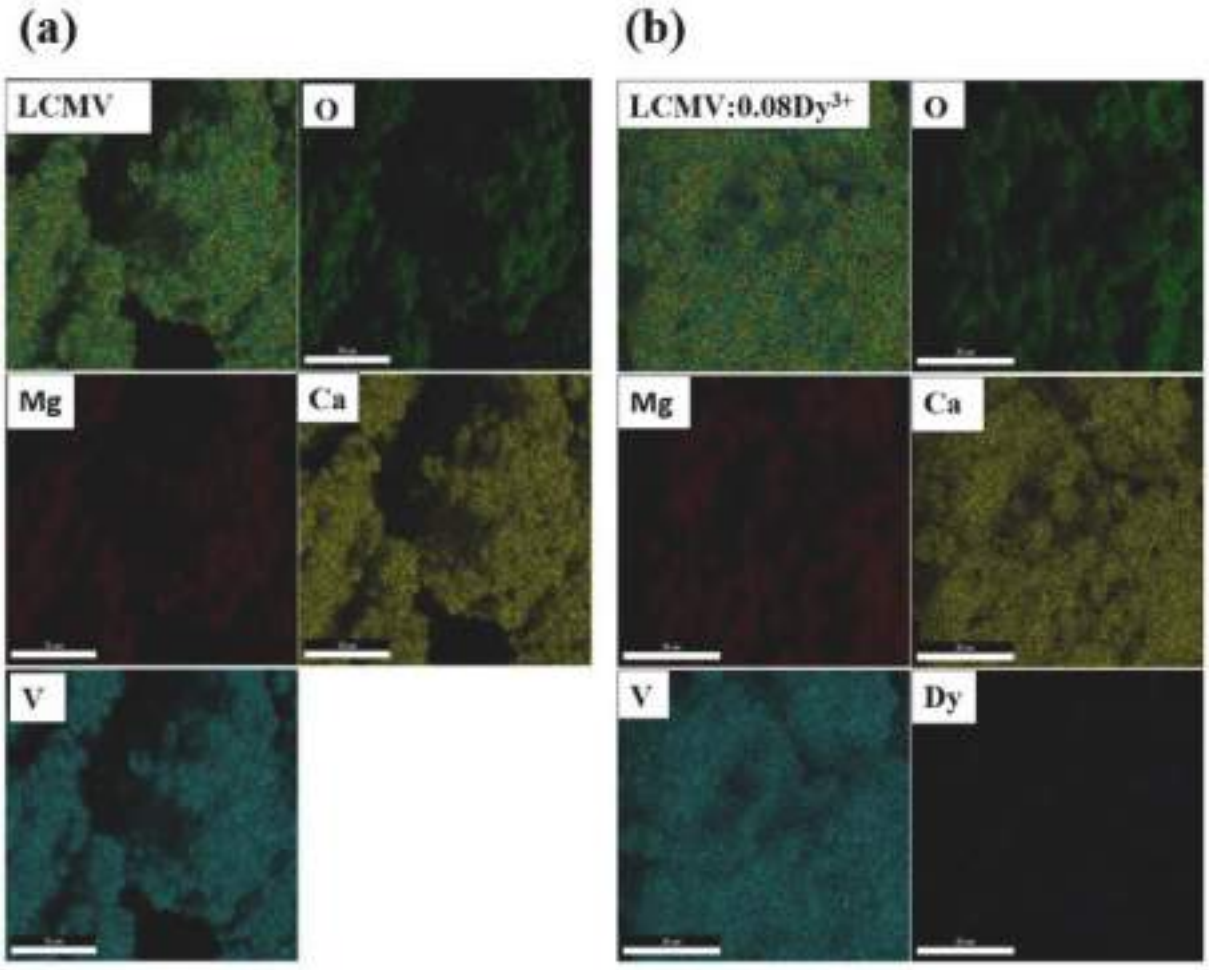

Fig. 4. (a) Elemental mapping of $LiCa_2Mg_2V_3O_{12}$ phosphor **(b)** Elemental mapping of $LiCa_2Mg_2V_3O_{12}$:0.08Dy^{3+}phosphor.

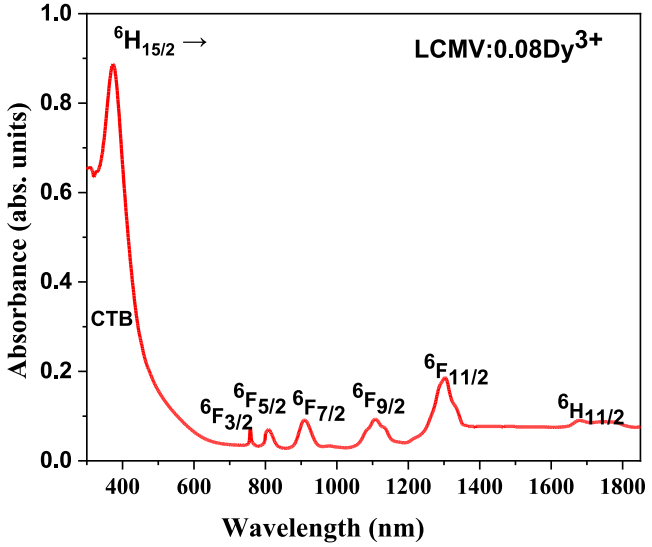

Fig. 5. UV–Vis–NIR absorption spectrum of $LiCa_2Mg_2V_3O_{12}$:0.08Dy^{3+} phosphor.

Ω_6 is structure dependent. The quality of fit between S_{meas} and S_{cal} is evaluated by root mean square deviation (σ) and the lower value of σ confirms the validity of J-O analysis.

Table 2
Determined values of the nephelauxetic ratio (β) and the bonding parameter (δ).

$^6H_{15/2}$ →	$^6H_{11/2}$	$^6F_{11/2}$	$^6F_{9/2}$	$^6F_{7/2}$	$^6F_{5/2}$	$^6F_{3/2}$
ν_c (cm^{-1})	5952	7680	9033	11013	12360	13192
ν_a (cm^{-1})	5833	7730	9087	11025	12432	13212
β	1.0204	0.9935	0.9940	0.9989	0.9942	0.9984
$\bar{\beta} = 0.9999$; $\delta = 0.0100$ (covalent bonding)						

3.3. Luminescence properties

3.3.1. Photoluminescence spectra

The PLE and PL spectra of undoped $LiCa_2Mg_2V_3O_{12}$ are shown in Fig. 9 (a-b). The $LiCa_2Mg_2V_3O_{12}$ phosphor exhibits a broad band emission spectrum that almost cover the entire visible region from 400 to 700 nm with a maximum at 513 nm. Meanwhile by fitting the spectra using Gaussian function two sub-bands at 2.55 and 2.34 eV are obtained which corresponds to the $^3T_2 \rightarrow {}^1A_1$ and $^3T_1 \rightarrow {}^1A_1$ transitions of $(VO_4)^{3-}$ groups. The $LiCa_2Mg_2V_3O_{12}$ phosphor shows a green emission at an excitation of 345 nm. The PLE spectra monitored at 513 nm shows an excitation band which covers the region 200–400 nm with peak at 345 nm. The deconvoluted sub-bands at 3.69 and 3.49 eV are ascribed to the $^1A_1 \rightarrow {}^1T_2$ and $^1A_1 \rightarrow {}^1T_1$ transitions [11]. The schematic representation of electron transition in $(VO_4)^{3-}$ is displayed in Fig. 9 (c).

The broad excitation band of $LiCa_2Mg_2V_3O_{12}$:0.08Dy^{3+} phosphor monitored at an emission wavelength of 576 nm and the PL emission spectra of phosphors at an excitation of 338 nm for different Dy^{3+}

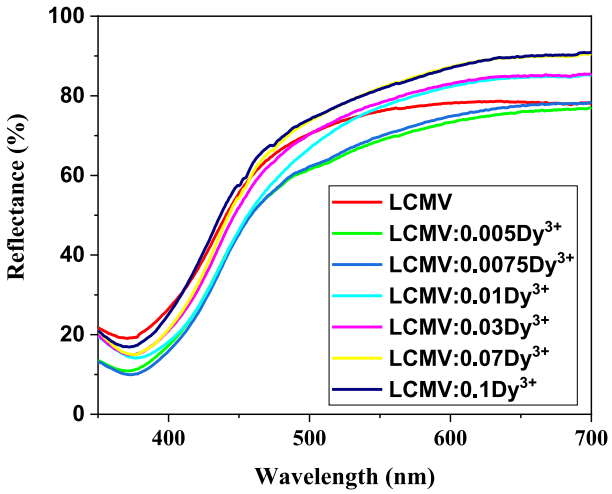

Fig. 6. Diffuse reflectance spectra of $LiCa_2Mg_2V_3O_{12}$:xDy^{3+} (x = 0, 0.005, 0.0075, 0.02, 0.04, 0.08, 0.1) phosphors.

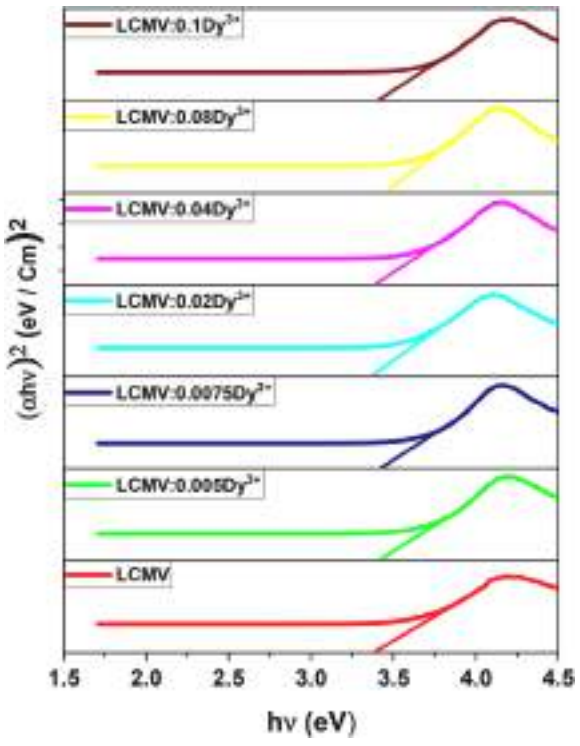

Fig. 7. Tauc plot of $LiCa_2Mg_2V_3O_{12}$:xDy^{3+} (x = 0, 0.005, 0.0075, 0.02, 0.04, 0.08, 0.1) phosphors.

concentrations are shown in Fig. 10 (a) & (b) respectively. The excitation spectra of $LiCa_2Mg_2V_3O_{12}$:$0.08Dy^{3+}$ phosphor consists of a wide band in the region 300–400 nm and have efficient absorption in UV region. The small excitation peaks at 385, 425, 449 and 476 nm are ascribed to the $^6H_{15/2} \rightarrow {}^4K_{17/2}$, $^6H_{15/2} \rightarrow {}^4G_{11/2}$, $^6H_{15/2} \rightarrow {}^4I_{15/2}$ and $^6H_{15/2} \rightarrow {}^4F_{9/2}$ transitions of Dy^{3+} [32].

The PL Spectra of $LiCa_2Mg_2V_3O_{12}$: xDy^{3+} (x = 0.005, 0.0075, 0.02, 0.04, 0.06, 0.08, 0.1) consists of peaks at 494 and 576 nm in addition to the broad band spectra of $LiCa_2Mg_2V_3O_{12}$. The peaks at 494 (blue) and 576 nm (yellow) are ascribed to the transitions $^4F_{9/2} \rightarrow {}^6H_{15/2}$ and $^4F_{9/2} \rightarrow {}^6H_{13/2}$ respectively [22]. The magnetic dipole allowed transition $^4F_{9/2} \rightarrow {}^6H_{15/2}$ with selection rule $\Delta J = 0, \pm 1$ is less sensitive to the host and barely changes with coordination environment or crystal field

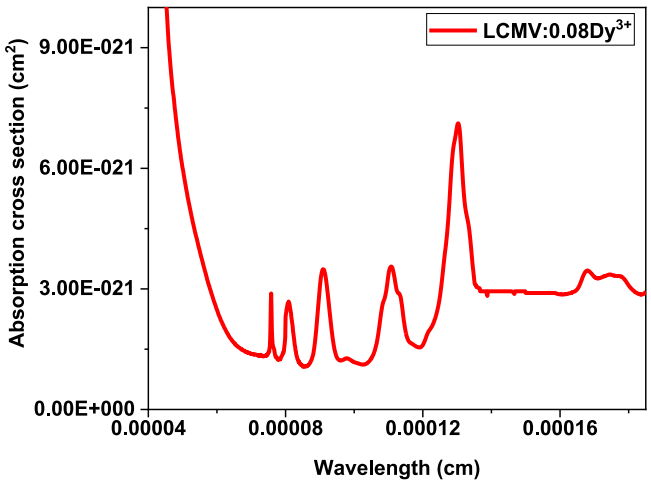

Fig. 8. Absolute absorption cross section of $LiCa_2Mg_2V_3O_{12}$:$0.08 Dy^{3+}$ phosphor.

strength. The blue emission corresponding to the transition $^4F_{9/2} \rightarrow {}^6H_{15/2}$ will show intense emission, when Dy^{3+} ions occupies in high symmetry sites having an inversion symmetry. The yellow emission ($^4F_{9/2} \rightarrow {}^6H_{13/2}$) due to the electric dipole allowed transition with selection rule $\Delta L = \pm 2$ and $\Delta J = 0$ or ± 2 occurs only when Dy^{3+} ions are in low symmetry sites without inversion center. The hypersensitive transition $^4F_{9/2} \rightarrow {}^6H_{13/2}$ strongly depends on the host environment. Thus the yellow to blue ratio can be used as the local field sensor to study the coordination environment of Dy^{3+}. The yellow/blue ratio of phosphors are found to be 0.77, 0.84, 0.84, 0.89, 0.95, 0.96 and 0.94 respectively. The higher value of yellow/blue ratio indicate higher degree of covalence and is consistent with J-O results [42]. For various concentrations of Dy^{3+}, the emission spectra have similar emission profiles, except for emission intensities. As the concentration of Dy^{3+} increases the emission of both $(VO_4)^{3-}$ group and Dy^{3+} initially increased and reached maximum when x = 0.08. As Dy^{3+} concentration increases beyond x = 0.08, the emission intensity drops due to the concentration quenching effect [25]. The variation of emission intensity of $^4F_{9/2} \rightarrow {}^6H_{15/2}$ and $^4F_{9/2} \rightarrow {}^6H_{13/2}$ transitions with Dy^{3+} concentration is shown in Fig. 10 (c). Moreover, to prove that concentration quenching effect guided to the decrease in Dy^{3+} emission, the critical distance R_c of donor and acceptor is evaluated by the following equation [28]:

$$R_c = 2\left(\frac{3V}{4\pi X_c N}\right)^{1/3} \tag{12}$$

where V represents the unit cell volume, X_c is the critical concentration and N is the number units. For $LiCa_2Mg_2V_3O_{12}$:$0.08Dy^{3+}$ phosphor the unit cell volume (V) is calculated to be 1908.3543 $Å^3$ and the values of X_c and N taken as 0.08 and 8 respectively. The critical distance R_c is determined to be 17.8607 Å. The non-radiative energy transfer of luminescence centers can be explained effectively by the exchange interaction and the multipolar interactions. Here the electric multipolar interaction prevailed as the critical distance R_c for exchange interaction should be less than 5 Å [28].

The nature of multipolar interaction can be further estimated by the equation:

$$\frac{\tau_0}{\tau} = C^{\theta/3} \tag{13}$$

where τ_0 represents intrinsic lifetime of Dy^{3+}, τ is the lifetime of Dy^{3+} at different concentration, C is the Dy^{3+} concentration, and the values θ = 6, 8, 10 ascribed to dipole-dipole (d-d), dipole-quadrupole (d-q), quadrupole-quadrupole (q-q) interactions, respectively. The different interaction mechanism plots are shown in Fig. 11 (a-c). The goodness of

Table 3
Calculated and measured line strengths of $LiCa_2Mg_2V_3O_{12}$:0.08 Dy^{3+} phosphor.

Transitions $^6H_{15/2}$ →	$U^{(2)}$	$U^{(4)}$	$U^{(6)}$	Wavelength (nm)	S_{meas} 10^{-20} cm^2	S_{cal} 10^{-20} cm^2	ΔS cm^2
$^6H_{11/2}$	0.0923	0.0366	0.6410	1680	1.5380	1.3845	0.1535
$^6F_{11/2}$	0.9387	0.8292	0.2048	1302	3.3539	3.3688	−0.0149
$^6F_{9/2}$	0.0000	0.5736	0.7213	1107	1.9549	1.8913	0.0636
$^6F_{7/2}$	0.0000	0.1360	0.7146	908	1.1955	1.4126	−0.2171
$^6F_{5/2}$	0.0000	0.0000	0.3452	809	0.6295	0.6122	0.0173
$^6F_{3/2}$	0.0000	0.0000	0.0610	758	0.2416	0.1081	0.0173

$\sigma = 0.1122 \times 10^{-20}$, $\Omega_2 = 2.2594 \times 10^{-20}$ cm^2, $\Omega_4 = 1.0669 \times 10^{-20}$ cm^2, $\Omega_6 = 1.7737 \times 10^{-20}$ cm^2, $\chi = 0.60155$

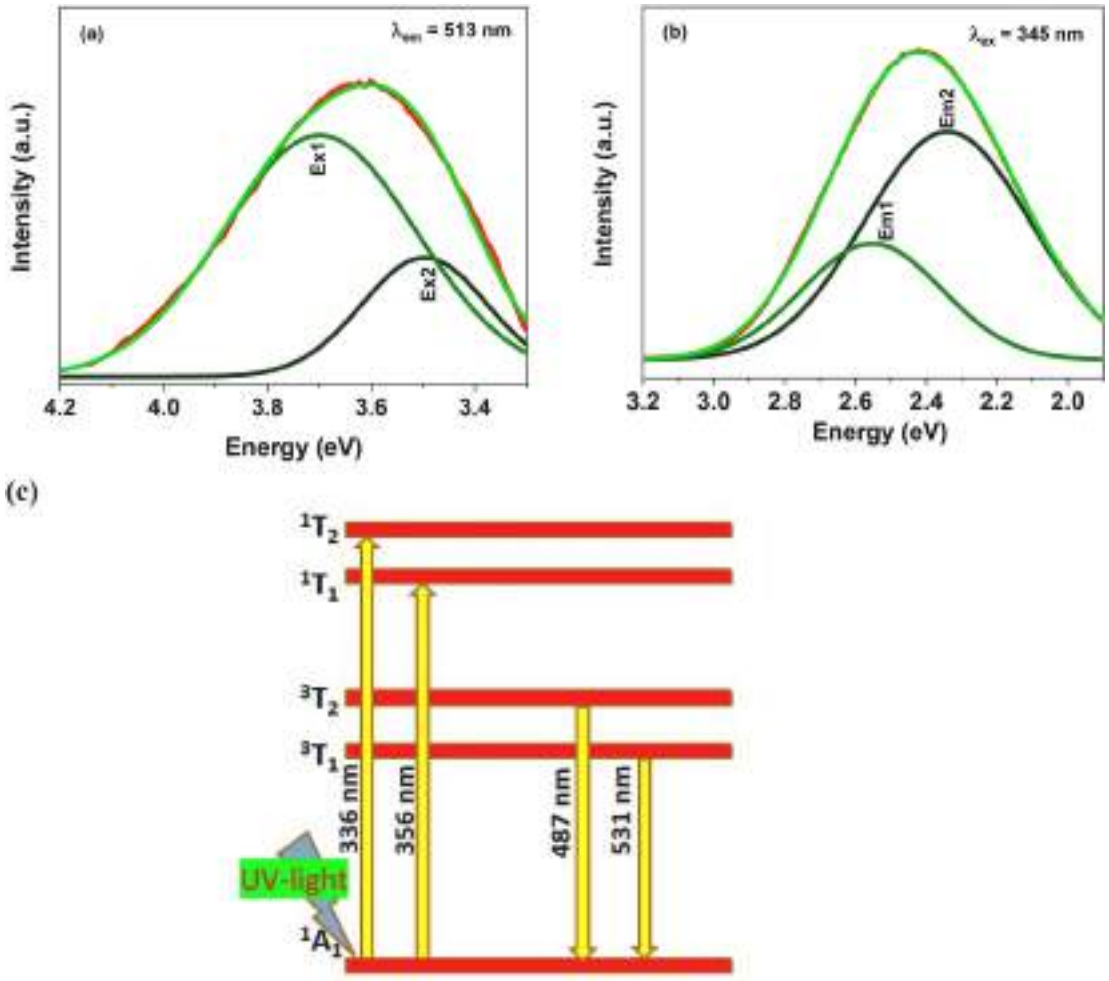

Fig. 9. (a) Excitation spectra of $LiCa_2Mg_2V_3O_{12}$ phosphor **(b)** Emission spectra of $LiCa_2Mg_2V_3O_{12}$ phosphor **(c)** The schematic representation of electron transition in $(VO_4)^{3-}$.

fit for $\alpha = 6$, 8 and 10 is $R^2 = 0.9887$, 0.9790 and 0.9587 respectively, which indicates that the dipole-dipole interaction is responsible for the concentration quenching in $LiCa_2Mg_2V_3O_{12}$:xDy^{3+} phosphor [3]. The corresponding energy transfer mechanism from $(VO_4)^{3-}$ to Dy^{3+} is represented in Fig. 11 (d). The quantum yield of $LiCa_2Mg_2V_3O_{12}$:0.08Dy^{3+} phosphor is found to be 31.40%. The excitation and emission spectra of $LiCa_2Mg_2V_3O_{12}$:0.08Dy^{3+} phosphor with respect to $BaSO_4$ reference is shown in Fig. 12.

3.3.2. *Radiative parameters*

The radiative parameters of $LiCa_2Mg_2V_3O_{12}$:0.08Dy^{3+} phosphor can be obtained by combining the J-O parameters calculated from the absorption spectra with the emission spectra. For a particular transition from ground state to excited state, the radiative transition probability is the sum of electric dipole and magnetic dipole transitions and is given by Ref. [34]:

$$A_R = A_{ed} + A_{md} \tag{14}$$

$$= \frac{64\pi^4}{3h\lambda^3(2J+1)} \left[\frac{n(n^2+2)^2}{9} S_{ed} + n^3 S_{md}\right] \tag{15}$$

where $\frac{n(n^2+2)^2}{9}$ and n^3 are the local field correction for electric and magnetic dipole emission transition respectively [40], S_{ed} and S_{md} represents the line strengths of electric and magnetic dipole transitions and is represented by the expressions [43,44]:

$$S_{ed} = e^2 \sum_{\lambda=2,4,6} \Omega_\lambda \left|\langle (S,L)J \| U^{(t)} \| (S',L')J' \rangle\right|^2 \tag{16}$$

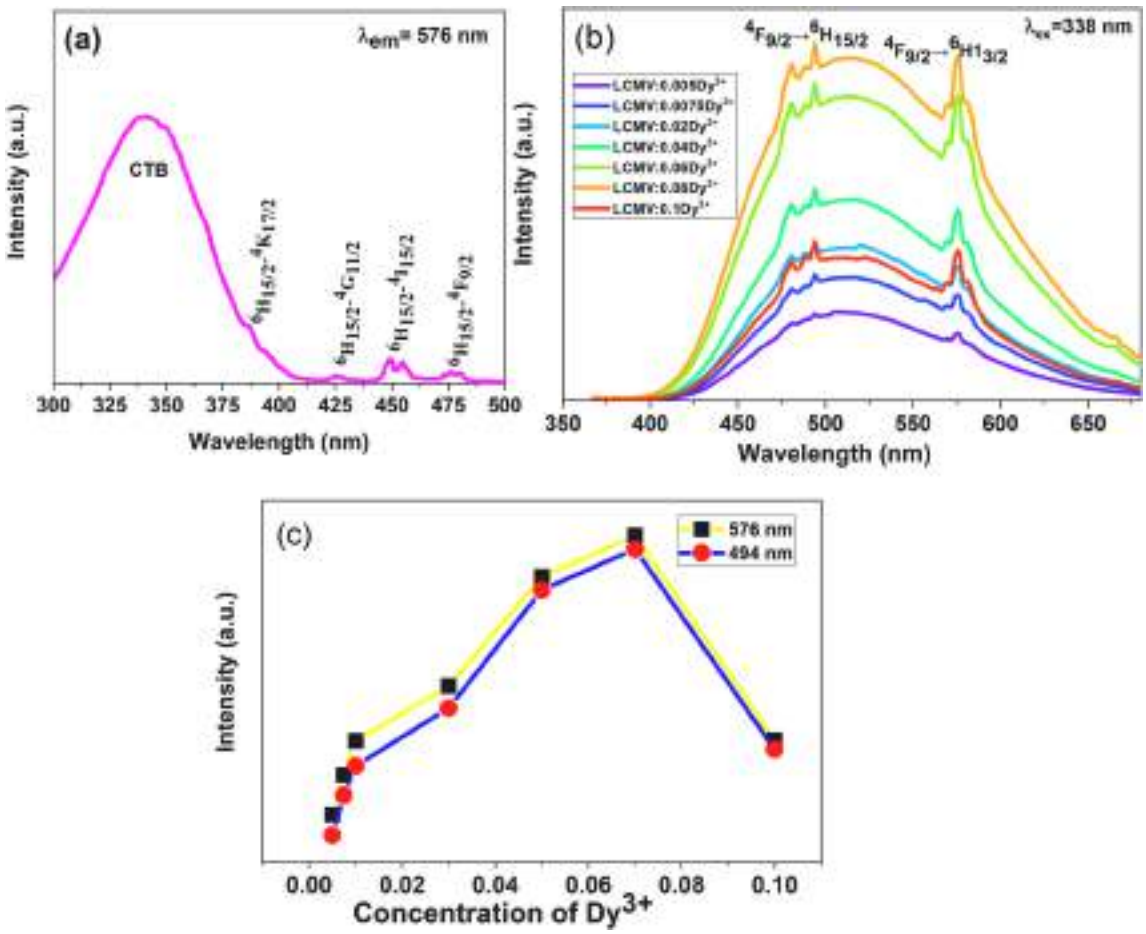

Fig. 10. (a). The excitation spectra of $LiCa_2Mg_2V_3O_{12}$:0.08Dy^{3+} phosphor **(b)** The emission spectra of $LiCa_2Mg_2V_3O_{12}$:xDy^{3+} (x = 0.005, 0.0075, 0.02, 0.04, 0.06, 0.08, 0.1) phosphor **(c)** Emission intensity variation of $^4F_{9/2} \rightarrow {}^6H_{15/2}$ and $^4F_{9/2} \rightarrow {}^6H_{13/2}$ transitions with Dy^{3+} concentration.

$$S_{md} = \mu_B^2 |\langle (S,L)J \| L + 2S \| (S',L')J' \rangle|^2 \quad (17)$$

where $\mu_B = \frac{h}{4\pi mc}$.

The total radiation transition probability A_T is given by the formula:

$$A_T = \sum A_R (J' \rightarrow J) \quad (18)$$

The predicted radiative life time (τ_{rad}) and the branching ratio (β_R) can be estimated using following expressions respectively [40]:

$$\tau_{rad} = \frac{1}{\sum A_R(J' \rightarrow J)} \quad (19)$$

$$\beta_R = \frac{A_R(J' \rightarrow J)}{\sum A_R(J' \rightarrow J)} \quad (20)$$

The stimulated emission cross section (σ_e) for a particular transition is obtained by Ref. [44]:

$$\sigma_e = \frac{\lambda_P^4 A_R (J' \rightarrow J)}{8\pi\, Cn^2 \Delta\lambda_{eff}} \quad (21)$$

where λ_P, $\Delta\lambda_{eff}$ and c are the peak wavelength of emission band, effective line width of transition and the velocity of light respectively.

The radiative transition probability (A_R), branching ratio (β_R), stimulated emission cross-section (σ_e), gain bandwidth ($\sigma_e \times \Delta\lambda_{eff}$) and optical gain ($\sigma_e \times \tau_R$) for the Dy^{3+} doped $LiCa_2Mg_2V_3O_{12}$ phosphor are calculated and is listed in Table 4. The maximum transition probability of phosphor is at 576 nm corresponding to $^4F_{9/2} \rightarrow {}^6H_{13/2}$ transition and the radiative lifetime is found to be 5.58 μs. The maximum radiative branching ratio of 13.49 is exhibited by the $^4F_{9/2} \rightarrow {}^6H_{13/2}$ transition. The experimental branching ratio is estimated using the relative area of emission bands and is 0.6980 for $^4F_{9/2} \rightarrow {}^6H_{13/2}$ transition. The discrepancy between calculated and experimental branching ratio is due to the non-radiative transitions from $^4F_{9/2}$ level of Dy^{3+} in the $LiCa_2Mg_2V_3O_{12}$:0.08 Dy^{3+} host. The higher value of stimulated emission cross-section (σ_e) of $^4F_{9/2} \rightarrow {}^6H_{13/2}$ transition aids for low threshold and is a good candidate for optoelectronic applications. The elevated value of gain bandwidth ($\sigma_e \times \Delta\lambda_{eff}$) and optical gain ($\sigma_e \times \tau_R$) suggest that the $LiCa_2Mg_2V_3O_{12}$:0.08 Dy^{3+} phosphor can be used as a good optical amplifier [33].

3.3.3. CIE diagram

The PL emission color of $LiCa_2Mg_2V_3O_{12}$:x Dy^{3+} (x = 0, 0.005, 0.0075, 0.02, 0.04, 0.06, 0.08 and 0.1) phosphors are evaulated by Commision Internationale de L'Eclairage (1931). The CIE chromaticity coordinates of phosphors excited at 338 nm are shown in Fig. 13 (a). The power spectrum of $LiCa_2Mg_2V_3O_{12}$:0.08Dy^{3+} phosphor is shown in Fig. 13 (b). The correlated color temperature (CCT) of phosphors are

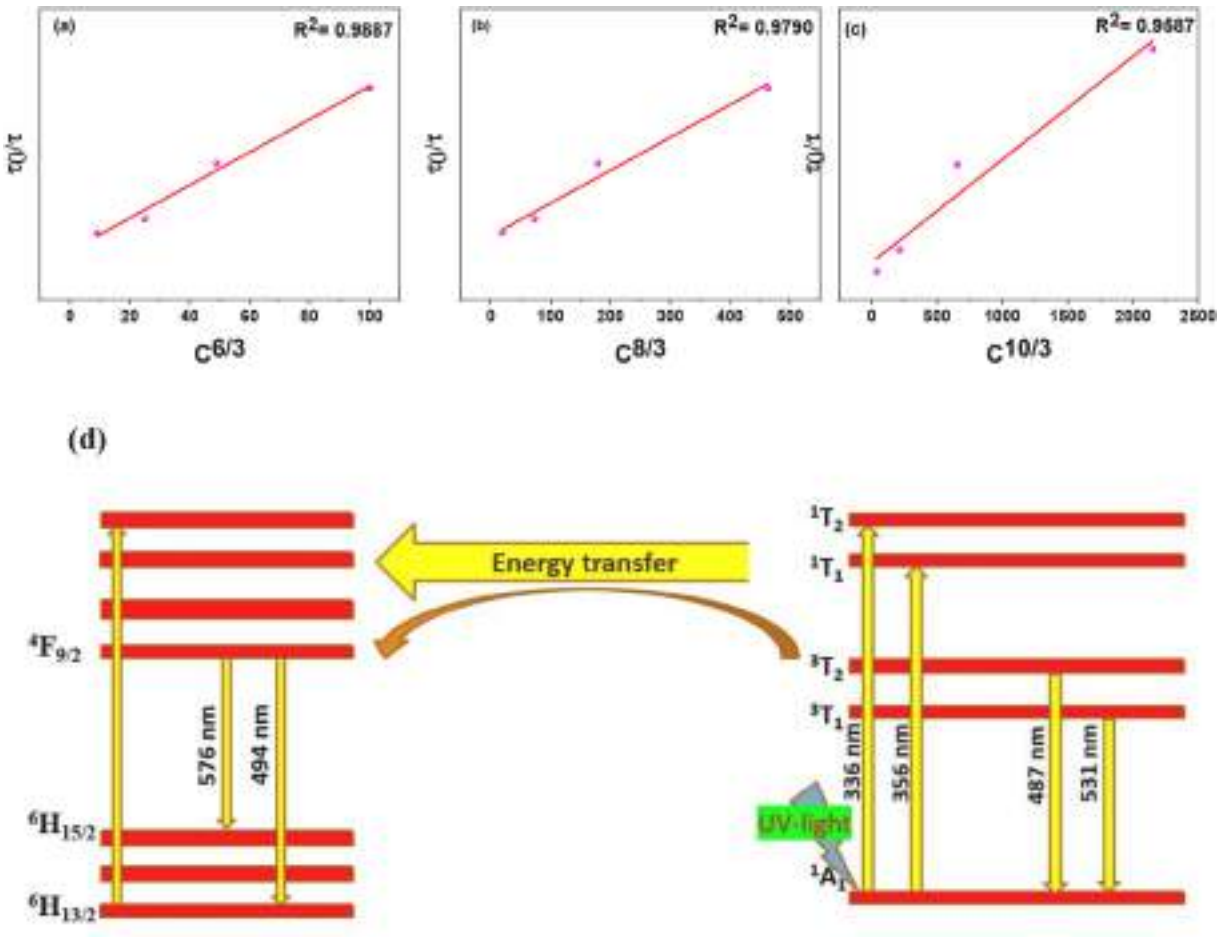

Fig. 11. (a) Dipole-dipole **(b)** Dipole-quadropole and **(c)** Quadropole-quadropole interaction mechanism **(d)** Energy transfer mechanism from $(VO_4)^{3-}$ to Dy^{3+}.

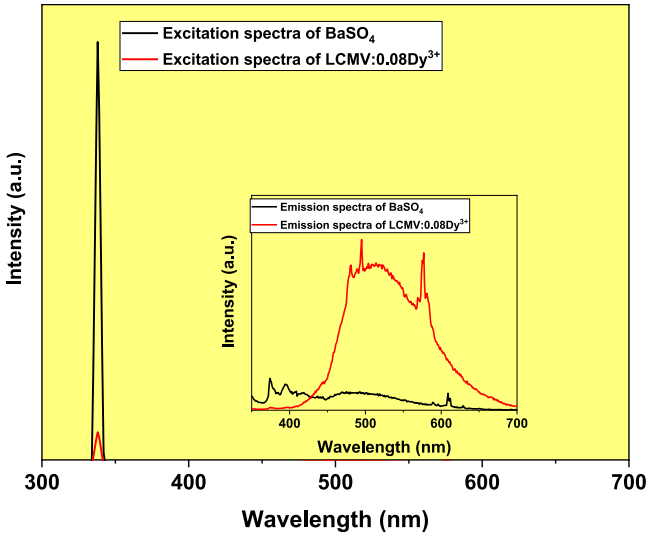

Fig. 12. The excitation and emission spectra of $LiCa_2Mg_2V_3O_{12}$:0.08Dy^{3+} phosphor with respect to $BaSO_4$ reference.

estimated from McCamy empirical formula [45]:

$$CCT = -449n^3 + 3525n^2 - 6823.3n + 5520.33 \quad (22)$$

where, $n = \frac{x-x_e}{y-y_e}$, $x_e = 0.3320$ $y_e = 0.1858$, (x,y) are the CIE coordinates of phosphors. The color purity of phosphors is calculated using the following equation [45]:

Table 4
Radiative parameters of $LiCa_2Mg_2V_3O_{12}$:0.08Dy^{3+} phosphor.

Radiative properties	$^4F_{9/2} \rightarrow {}^6H_{15/2}$	$^4F_{9/2} \rightarrow {}^6H_{13/2}$
Peak wavelength, λ (nm)	495	576
Effective bandwidth, $\Delta\lambda_{eff}$ (nm)	5	8
Spontaneous probability, A_R (s^{-1})	540.65 × 10^2	1250.04 × 10^2
Radiative branching ratio, β_R	6.31	13.49
Experimental branching ratio, β_R	0.3019	0.6980
Stimulated emission cross-section, σ_e (× $10^{-20}$$cm^2$)	16.00	98.37
Gain bandwidth, $\sigma_e \times \Delta\lambda_{eff}$ (× 10^{-28} cm^3)	8.00	78.69
Optical gain, $\sigma_e \times \tau_R$ (× 10^{-25} cm^2 s)	8.93	54.95

$$\text{Color purity} = \frac{\sqrt{(x-x_{ee})^2 + (y-y_{ee})^2}}{\sqrt{(x_d-x_{ee})^2 + (y_d-y_{ee})^2}} \quad (23)$$

where (x,y), (x_{ee}, y_{ee}) and (x_d y_d) are chromaticity coordinate, equal energy white coordinate and dominant wavelength coordinate respectively. The CIE coordinates, CCT values and color purity are listed in Table 5. From the color coordinates it is evident that the prepared phosphors exhibits near white emission with color purity close to the standard white light color purity (0%) [35]. Fig. 13 (c) shows the color of $LiCa_2Mg_2V_3O_{12}$:0.08Dy^{3+} phosphor at normal day light and UV- 395 nm irradiation. The CCT values of doped phosphors are between 6000 and 7000K, which is higher than the CCT value of fluorescent tube

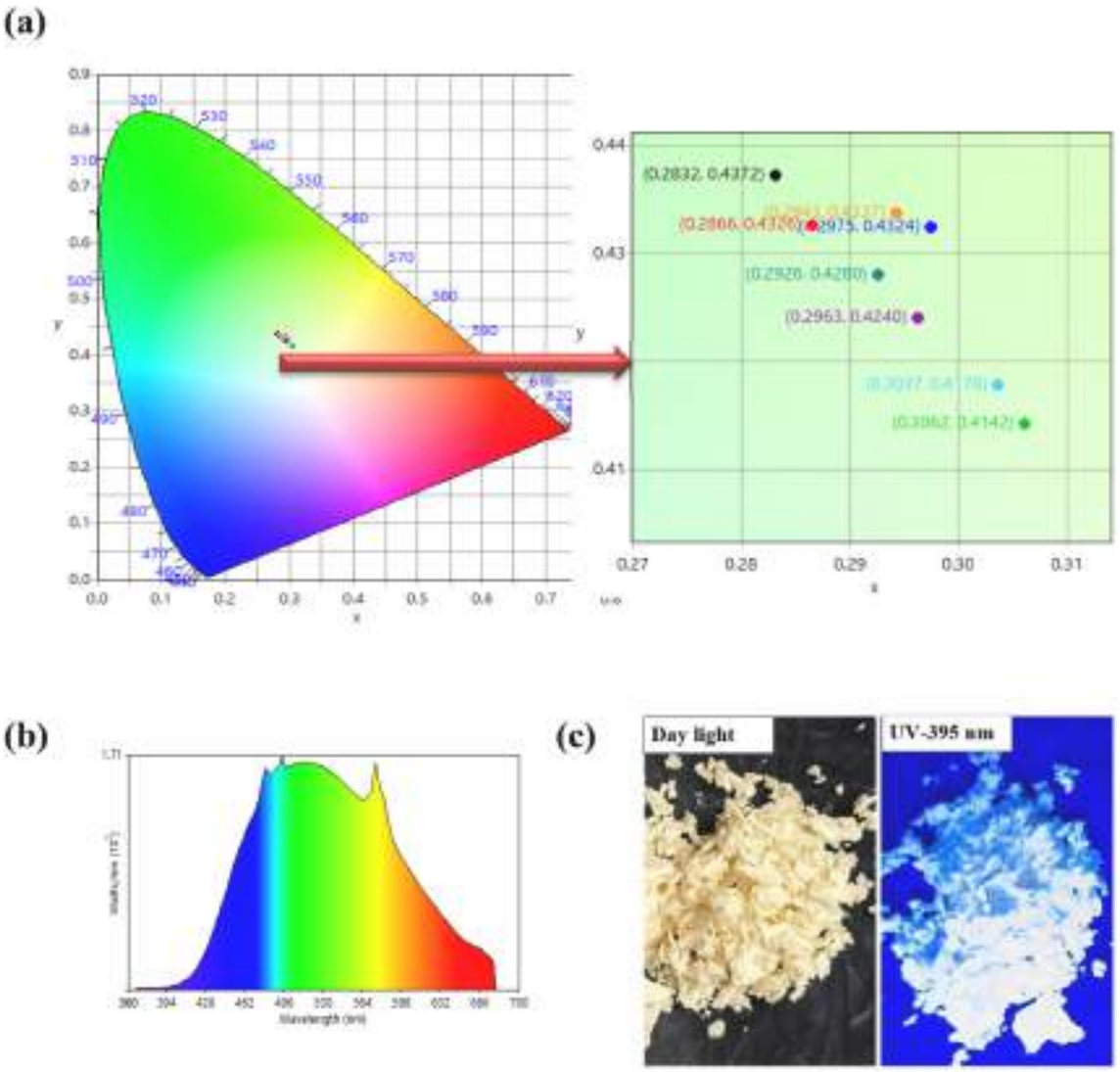

Fig. 13. (a) CIE chromaticity coordinates of $LiCa_2Mg_2V_3O_{12}$:xDy^{3+} (x = 0, 0.005, 0.0075, 0.02, 0.04, 0.06, 0.08, 0.1) phosphors **(b)** Power spectrum of $LiCa_2Mg_2V_3O_{12}$:$0.08Dy^{3+}$ **(c)** color of $LiCa_2Mg_2V_3O_{12}$:$0.08Dy^{3+}$ phosphor at normal day light and UV- 395 nm irradiation.

Table 5
CIE Coordinates, CCT values and color purity of $LiCa_2Mg_2V_3O_{12}$:xDy^{3+} (x = 0, 0.005, 0.0075, 0.02, 0.04, 0.06, 0.08, 0.1) phosphors.

Sample	(x,y)	CCT (K)	Color purity (%)
LCMV	(0.2832, 0.4372)	6974	7.39
LCMV:0.005Dy^{3+}	(0.2975, 0.4324)	6545	6.75
LCMV:0.0075Dy^{3+}	(0.2866, 0.4326)	6897	6.97
LCMV:0.02Dy^{3+}	(0.2943, 0.4337)	6640	6.90
LCMV:0.04Dy^{3+}	(0.2926, 0.4280)	6724	6.60
LCMV:0.06Dy^{3+}	(0.2963, 0.4240)	6623	6.27
LCMV:0.08Dy^{3+}	(0.3037, 0.4178)	6405	5.74
LCMV:0.1Dy^{3+}	(0.3062, 0.4142)	6319	5.47

(3935 K) and lower than the CCT value of fluorescent lamp (7200–8500 K). The present phoshor material emission is very close to natural light, and find applications in exhibition window, reading room of library, etc [46].

3.3.4. Life time analysis and quantum efficiency

The luminescence decay curves of $LiCa_2Mg_2V_3O_{12}$:xDy^{3+} phosphors at room temperature (λ_{ex} = 338 nm and λ_{em} = 576 nm) are displayed in Fig. 14 (a) & (b). The decay curves could be well fitted by using single-exponential function as follows [3]:

$$I(t) = A^*\exp(-t/\tau) \quad (24)$$

where I(t) is the photoluminescence intensity at time t, A and τ are weight factor and life time respectively. Based on fitting, the life time of $LiCa_2Mg_2V_3O_{12}$ phosphors with various Dy^{3+} concentration (x = 0, 0.0075, 0.02, 0.03, 0.06, 0.08 and 0.1) is found to be 4.4055, 4.3110, 4.2025, 4.1028, 4.0918, 4.0486 and 3.9916 μs respectively. Here the lifetime of phosphors decreases with increase in Dy^{3+} concentration is due to the non-radiative energy transfer and self absorption rate among Dy^{3+} [3]. The disparity between the experimental lifetime (τ_{exp}) and calculated lifetime (τ_{calc}) of $LiCa_2Mg_2V_3O_{12}$:$0.08Dy^{3+}$ phosphor is attributed to the manifestation of non-radiative relaxation process and can be expressed as follows [35]:

$$W_{NR} = \tau_{exp}^{-1} - \tau_{calc}^{-1} \quad (25)$$

The value of W_{NR} is obtained to be 1.54 μs. The intrinsic quantum efficiency of luminescence systems are evaluated as the ratio of number of photons emitted to number of photons absorbed. For rare earth doped systems, the luminescence intrinsic quantum efficiency (Ƞ) can be calculated as the ratio of experimental life time (τ_{exp}) to calculated lifetime (τ_{calc}) as given in equation [35,47]:

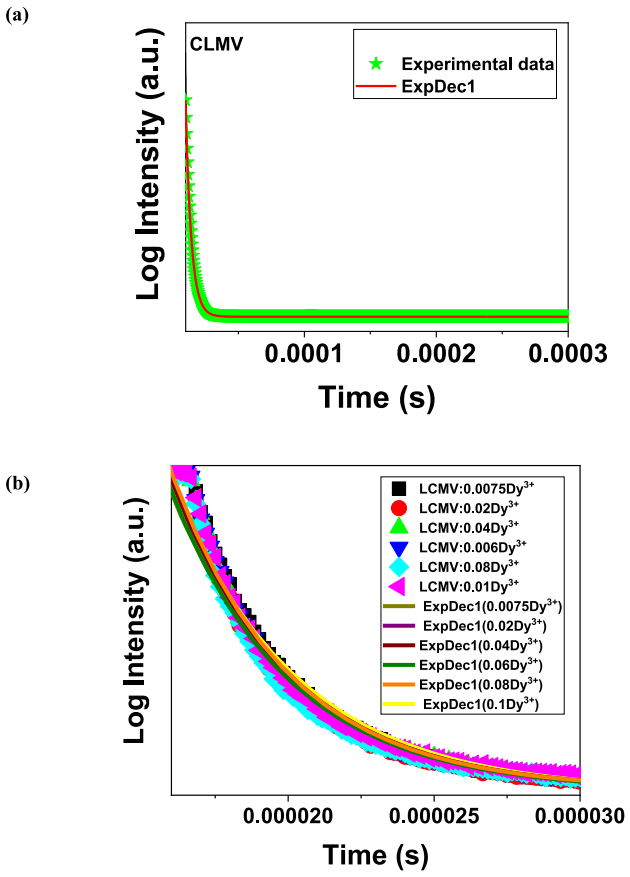

Fig. 14. The luminescence decay analysis curves of $LiCa_2Mg_2V_3O_{12}$: xDy^{3+} **(a)** x = 0, **(b)** x = 0.0075, 0.02, 0.04, 0.06, 0.08 and 0.1 phosphors.

$$\eta = \frac{\tau_{exp}}{\tau_{calc}} \times 100\ \% \tag{26}$$

The intrinsic quantum efficiency of present system is calculated to be 72.46%, which is much better value than the previously reported white light emitting phosphors like Dy^{3+} doped $Gd(P_xV_{1-x})\ O_4$ [48].

3.4. Thermo sensor application of $LiCa_2Mg_2V_3O_{12}$:0.08Dy^{3+} phosphor

The thermal stability of $LiCa_2Mg_2V_3O_{12}$:0.08Dy^{3+} phosphor is analyzed by the temperature dependent emission spectra recorded at an excitation wavelength of 338 nm. The temperature dependent PL spectra of phosphor in heating and cooling process is shown in Fig. 15 (a) & (b). It is noted that the emission intensity of VO_4^{3-} group and Dy^{3+} decreases with increase in temperature. The fall in emission intensity is caused by the thermal quenching process due to the non-radiative transitions that prevails at high temperatures. Furthermore, the relationship between emission intensity and temperature of non-thermally coupled levels (NTCLs) are adhering to the Arrhenius equation and the activation energy of emission centers can be estimated using the following equation [17,49–51]:

$$I = \frac{I_0}{1 + A\ exp(-\Delta E/kT)} \tag{27}$$

where I and I_0 are the emission intensity at temperature T and initial intensity respectively, A is a constant, ΔE is activation energy and k is Boltzmann's constant (k = 0.695 $cm^{-1}K^{-1}$) [52]. The activation energy is obtained from the slope of curve $1/kT$ versus $\ln(I_0/I_T - 1)$ as displayed in Fig. 15 (c) and (d). The activation energies of emission centers VO_4^{3-} and Dy^{3+} in $LiCa_2Mg_2V_3O_{12}$:0.08Dy^{3+} phosphor are 2341.64 cm^{-1} (0.29 eV) and 2668.21 cm^{-1} (0.33 eV) respectively [31]. Therefore, the PL emission intensity of VO_4^{3-} group decreases faster than that of Dy^{3+}.

The diverse thermal response of VO_4^{3-} group and Dy^{3+} can be employed for the practical application of temperature sensing. The fluorescence intensity ratio (FIR) of NTCLs can be estimated using the following equation [2,17,49,50,53,54]:

$$FIR = \frac{I_{Dy^{3+}}}{I_{VO_4^{3-}}} = \frac{I_{0,Dy^{3+}}}{I_{0,VO_4^{3-}}} \frac{1 + A_{VO_4^{3-}} \exp\left(-\Delta E_{VO_4^{3-}}/kT\right)}{1 + A_{Dy^{3+}} \exp\left(-\Delta E_{Dy^{3+}}/kT\right)} \approx B + C \exp(-E/kT) \tag{28}$$

where B, C and E are parameters corresponding to the I_0, A and ΔE of Dy^{3+} ions to the VO_4^{3-} group. The temperature dependent FIR plot of $LiCa_2Mg_2V_3O_{12}$:0.08Dy^{3+} phosphor is shown in Fig. 16 (a). The FIR values are calculated by determining the integrated emission intensity of VO_4^{3-} (513 nm) and Dy^{3+} (576 nm), whose integral intervals are [500, 564] and [570, 584] respectively [2,17,31]. The fitting of FIR curve using equation (28) gives B, C and E/k values as 1.0157, 5.6321 and 1093.75 respectively.

The absolute sensitivity (S_a) and relative sensitivity (S_r) of $LiCa_2Mg_2V_3O_{12}$:0.08Dy^{3+} phosphor is evaluated in accordance with FIR plot using equations [17]:

$$S_a = \frac{d(FIR)}{dT} = C \exp(-E/kT) \times \left(E/kT^2\right) \tag{29}$$

$$S_r = \frac{1}{FIR}\frac{d(FIR)}{dT} \times 100\% = \frac{C \exp(-E/kT)}{B + C \exp(-E/kT)} \times \frac{E}{kT^2} \times 100\% \tag{30}$$

The variation of absolute and relative sensitivity with temperature is shown in Fig. 16 (b) and the maximum value of S_a and S_r are 0.0063 K^{-1} and 0.41% K^{-1} at 400 K respectively. The thermal repeatability of $LiCa_2Mg_2V_3O_{12}$:0.08Dy^{3+} phosphor is estimated through the evaluation of FIR in heating up and cooling down process. Fig. 16 (c) shows that the phosphor has good thermal repeatability. The temperature resolution (δT) can be obtained from the following expression [55]:

$$\delta T = \frac{1}{S_r}\frac{\delta FIR}{FIR} \tag{31}$$

where δFIR corresponds to the standard deviation of FIR in 3 consecutive cycles of heating and cooling. As displayed in Fig. 16 (d) the phosphor has temperature resolution of 0.1449 K at 400 K. In comparison with the reported Dy^{3+} doped materials (Table 6), the present system has wide range temperature sensing property. Thus, the phosphor is a better candidate for optical thermometry based on FIR.

4. Conclusions

$LiCa_2Mg_2V_3O_{12}$:x Dy^{3+} phosphors have been synthesized by solid-state reaction method. The XRD profiles confirm the cubic garnet structure (Ia-3d space group) of prepared phosphors. The FESEM analysis shows that the average grain size of phosphors varies between 6 and 9 μm. The EDX spectra verifies the elemental composition of undoped and doped phosphors and the elemental mapping provides the homogenous distribution of constituent elements on the surface of the phosphors. The nephelauxetic ratio and bonding parameter has been calculated from UV–Vis–NIR absorption spectrum and the positive value of bonding parameter indicates the covalency betweeen Dy^{3+} ligand and $LiCa_2Mg_2V_3O_{12}$ host. The band gap energy of phosphors have been obtained from diffuse reflectance spectra and falls in the range 3.36–3.43 eV. The Judd-Ofelt intensity parameters of $LiCa_2Mg_2V_3O_{12}$:0.08Dy^{3+} phosphor are extracted from NIR absorption spectra and is determined to be $\Omega_2 = 2.2594 \times 10^{-20}\ cm^2$, $\Omega_4 = 1.0669 \times 10^{-20}\ cm^2$, $\Omega_6 = 1.7737 \times 10^{-20}\ cm^2$. The higher value of Ω_2 manifests a higher degree of covalence. The emission spectra monitored at 338 nm consist of blue emission (494 nm) and yellow emission (576 nm) corresponding to the transitions $^4F_{9/2} \rightarrow {}^6H_{15/2}$ and $^4F_{9/2} \rightarrow {}^6H_{13/2}$ respectively. The

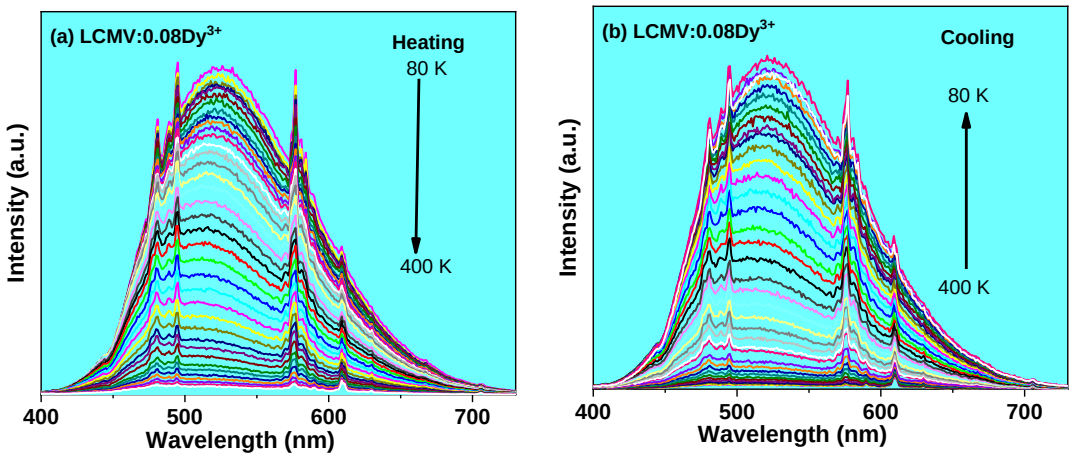

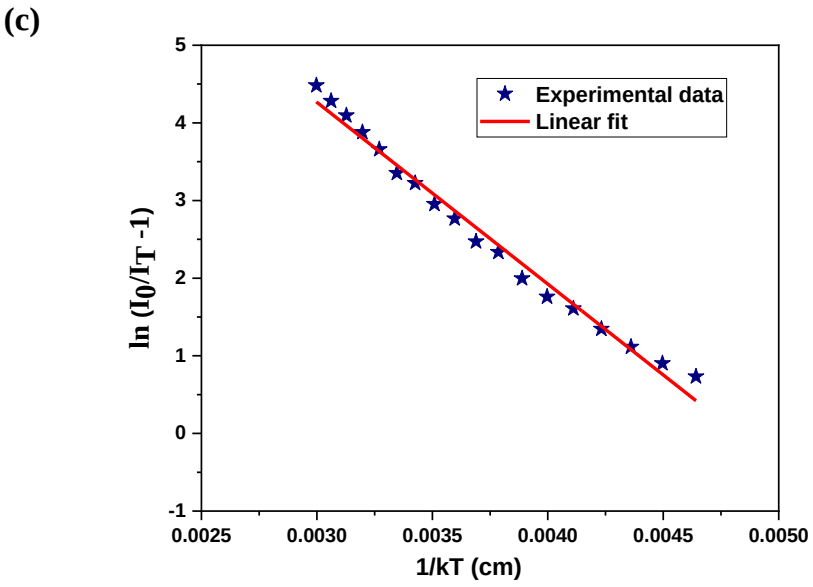

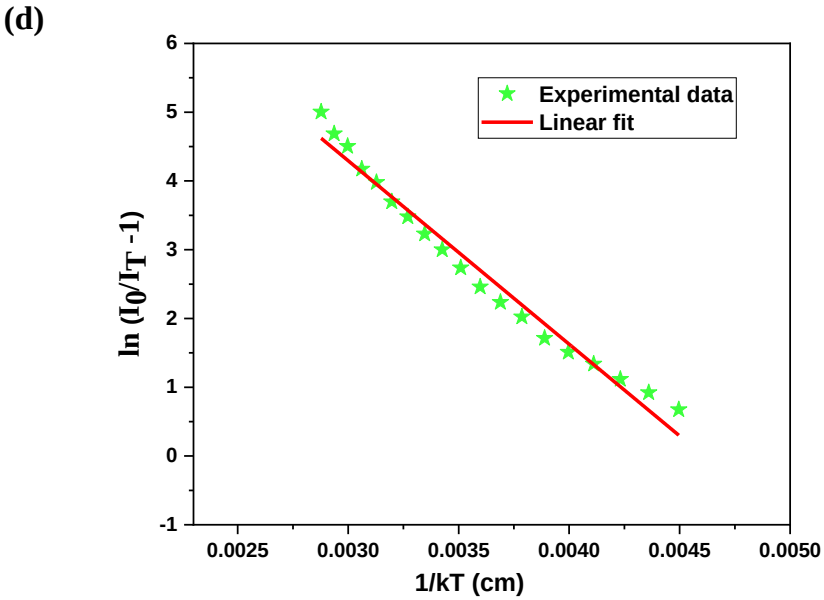

Fig. 15. (a) Temperature dependent PL spectra of $LiCa_2Mg_2V_3O_{12}$:0.08Dy^{3+} phosphor in Heating and **(b)** Cooling. Linear fit of Arrhenius plot of **(c)** VO_4^{3-} and **(d)** Dy^{3+} emission centers.

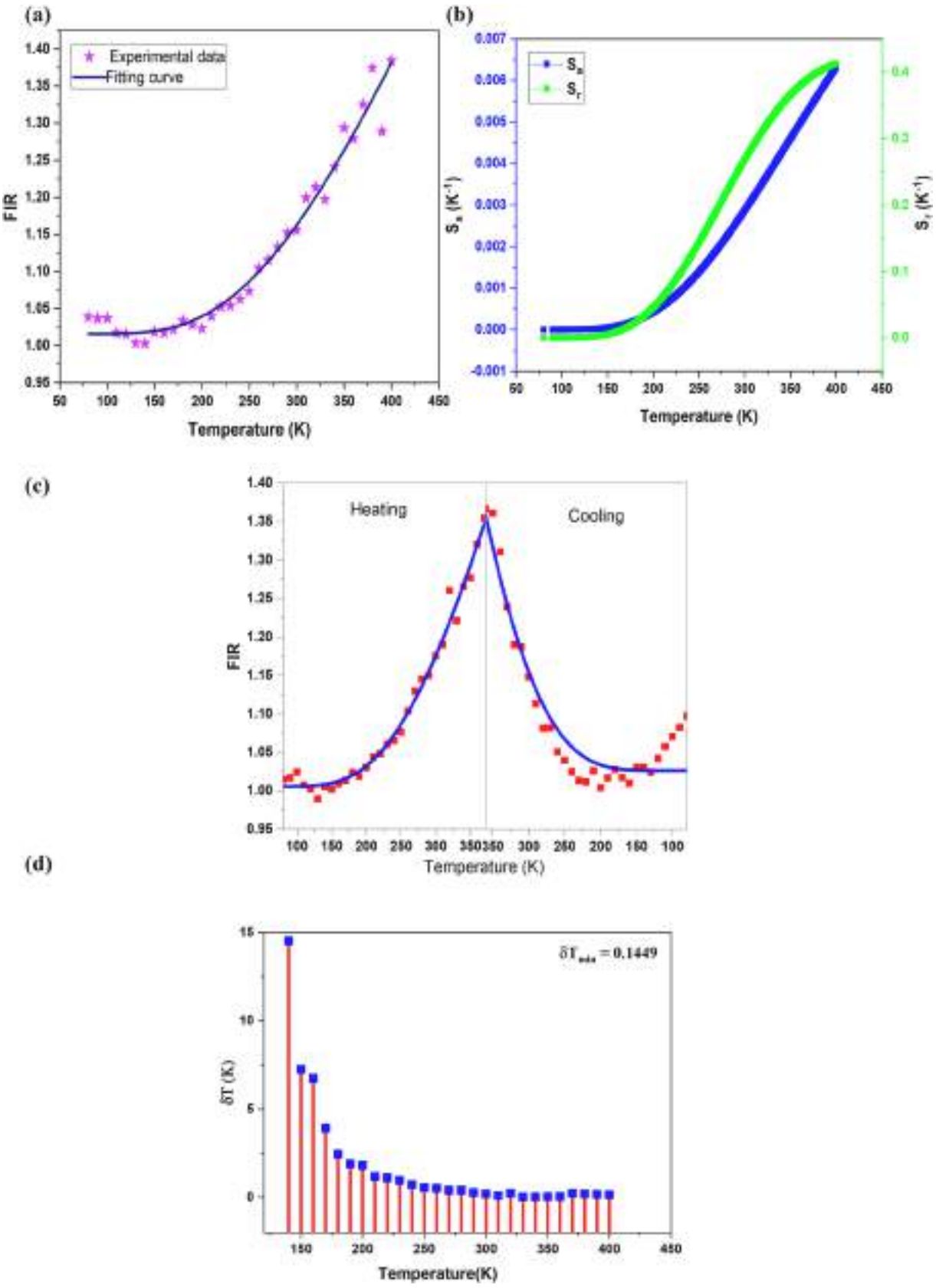

Fig. 16. **(a)** The temperature dependent FIR plot of $LiCa_2Mg_2V_3O_{12}$:0.08Dy^{3+} phosphor **(b)** Variation of absolute and relative sensitivity with temperature **(c)** FIR in heating up and cooling down process **(d)** Temperature resolution (δT) curve.

Table 6
Comparative study of temperature dependent luminescence properties of Dy^{3+} doped materials.

Material	Temperature range (K)	S_a-max (K^{-1})	S_r-max (% K^{-1})	Ref
$CaLa_4(SiO_4)_3O$: Dy^{3+}	298–548	0.00708 (at 548 K)	0.1673 (at 298 K)	[56]
$Sr_9Ga(PO_4)_7$: Dy^{3+}	298–598	0.018 (at 598 K)	0.87 (at 598 K)	[57]
$Ca_9Tb_xDy_{1x}(PO_4)_5(SiO_4)F_2$	303–573	0.0008809	0.003142	[58]
$LiY_9(SiO_4)_6O_2$: Ce^{3+}, Dy^{3+}	300–400	–	0.43 (at 400 K)	[59]
$LiCa_2Mg_2V_3O_{12}$:Dy^{3+}	80–400	0.0063	0.41 (at 400 K)	Present work

mechanism of concentration quenching is observed at 8 mol % of Dy^{3+} in $LiCa_2Mg_2V_3O_{12}$ host and is due to the dipole-dipole interaction. The energy transfer mechanism between the $(VO_4)^{3-}$ and Dy^{3+} is represented by the energy level diagram. The optimum concentration emission has high quantum yield of 31.40%. From the obtained J-O radiative parameters, the $LiCa_2Mg_2V_3O_{12}$:$0.08Dy^{3+}$ phosphor is identified to have higher values of stimulated emission cross section, gain bandwidth and optical gain for $^4F_{9/2} \rightarrow {}^6H_{13/2}$ transition and have attractive features for optical applications. The photometric parameters such as CIE chromaticity coordinates, CCT, color purity and Y/B intensity ratio have been examined in detail. The CIE chromaticity coordinate of the phosphor is in white region and thus find applications in WLEDs. The lifetime of $LiCa_2Mg_2V_3O_{12}$:xDy^{3+} phosphor decreases from 4.40 to 3.99 μs and the quantum efficiency of $LiCa_2Mg_2V_3O_{12}$:$0.08Dy^{3+}$ is found to be 72.46%. The fluorescence intensity ratio of phosphor with temperature shows that the phosphor have thermo-sensing property in the range 80–400 K. The maximum S_a and Sr values of phosphor are 0.0063 K^{-1} (at 400 K) and 0.41 K^{-1} (at 400 K) respectively. The thermal repeatability of phosphor shows good thermal stability and temperature resolution is found to be 0.1449 K. Thus, the present phosphor is a good candiate for optical amplifiers, visible lasers, thermo sensor and display applications.

CRediT authorship contribution statement

Raji R: Conceptualization, Methodology, Investigation, Validation, Formal analysis, Writing – original draft. **Anjana P.S:** Supervision, Resources, Formal analysis, Writing – review & editing. **Gopakumar N:** Supervision, Resources, Formal analysis, Writing – review & editing.

Declaration of competing interest

The authors declare that they have no known competing financial interests or personal relationships that could have appeared to influence the work reported in this paper.

Data availability

Data will be made available on request.

Acknowledgments

The authors acknowledge University of Kerala for financial support under University Junior Research Felloship. The authors are thankful to CLIF, University of Kerala for X-ray diffraction analysis, EDX-Elemental mapping, quantum yield and temperature dependent PL studies. The authors are grateful to Dr. K. G. Gopchandran, Department of Optoelectronics, University of Kerala for UV–Visible–NIR studies and FESEM analysis. The authors are thankful to SAIF, M.G University for photoluminescence and decay time analysis.

References

[1] S. Dutta, S. Som, S.K. Sharma, Excitation spectra and luminescence decay analysis of K^+ compensated Dy^{3+} doped $CaMoO_4$ phosphors, RSC Adv. 5 (2015) 7380–7387, https://doi.org/10.1039/c4ra12447b.
[2] H. Zhou, N. Guo, X. Lü, Y. Ding, L. Wang, R. Ouyang, B. Shao, Ratiometric and colorimetric fluorescence temperature sensing properties of trivalent europium or samarium doped self-activated vanadate dual emitting phosphors, J. Lumin. 217 (2020), 116758, https://doi.org/10.1016/j.jlumin.2019.116758.
[3] R. Cao, X. Wang, Y. Jiao, X. Ouyang, S. Guo, P. Liu, H. Ao, C. Cao, A single-phase $NaCa_2Mg_2V_3O_{12}$:Sm^{3+} phosphor: synthesis, energy transfer, and luminescence properties, J. Lumin. 212 (2019) 23–28, https://doi.org/10.1016/j.jlumin.2019.04.017.
[4] D.D. Ramteke, R.S. Gedam, H.C. Swart, Physical and optical properties of lithium borosilicate glasses doped with Dy^{3+} ions, Phys. B Condens. Matter 535 (2018) 194–197, https://doi.org/10.1016/j.physb.2017.07.035.
[5] S. Damodaraiah, V. Reddy Prasad, S. Babu, Y.C. Ratnakaram, Structural and luminescence properties of Dy^{3+} doped bismuth phosphate glasses for greenish yellow light applications, Opt. Mater. 67 (2017) 14–24, https://doi.org/10.1016/j.optmat.2017.03.023.
[6] X. Zhang, J. Zhang, X. Wu, L. Yu, Y. Liu, X. Xu, S. Lian, Discovery of blue-emitting Eu^{2+}-activated sodium aluminate phosphor with high thermal stability via phase segregation, Chem. Eng. J. 388 (2020), 124289, https://doi.org/10.1016/j.cej.2020.124289.
[7] L. Wang, C. Yuan, P. Hu, R. Li, Y. Liu, P. Sun, R. Dong, X. Qi, J. Jiang, H. Jiang, A low cost and high efficient $Ba_9(Lu_{2-x-y}Al_x)Si_6O_{24}$:$yCe^{3+}$ cyan-emitting phosphor, Ceram. Int. 46 (2020) 11466–11473, https://doi.org/10.1016/j.ceramint.2020.01.172.
[8] G.H. Li, N. Yang, J.G. Guo, Z.L. Wang, G.M. Cai, X.J. Wang, Efficient and stable $Sr_3Eu_2B_4O_{12}$ red phosphor benefiting from low symmetry and distorted local environment, Dalton Trans. 49 (2020) 3260–3271, https://doi.org/10.1039/c9dt04769g.
[9] H. Kaur, M. Jayasimhadri, Color tunable photoluminescence properties in Eu^{3+} doped calcium bismuth vanadate phosphors for luminescent devices, Ceram. Int. 45 (2019) 15385–15393, https://doi.org/10.1016/j.ceramint.2019.05.034.
[10] Y. Guo, S.H. Park, B.C. Choi, J.H. Jeong, J.H. Kim, Blue shift behavior of Eu^{2+} emission in eulytite-type $Sr_3La(PO_4)_3$ phosphor based on the release of adjacent Eu^{3+}-induced stress, J. Alloys Compd. 742 (2018) 159–164, https://doi.org/10.1016/j.jallcom.2018.01.281.
[11] X. Zhang, Z. Zhu, Z. Sun, Z. Guo, J. Zhang, Host-sensitized color-tunable luminescence properties of self-activated and Eu^{3+}-doped $Ca_3LiZnV_3O_{12}$ phosphors, J. Lumin. 203 (2018) 735–740, https://doi.org/10.1016/j.jlumin.2018.07.030.
[12] X. Chen, Z. Xia, Luminescence properties of $Li_2Ca_2ScV_3O_{12}$ and $Li_2Ca_2ScV_3O_{12}$:Eu^{3+} synthesized by solid-state reaction method, Opt. Mater. 35 (2013) 2736–2739, https://doi.org/10.1016/j.optmat.2013.06.008.
[13] H. Chen, J. Zhou, H. Zhang, Z. Hu, Broad-band emission and color tuning of Eu^{3+}-doped $LiCa_2SrMgV_3O_{12}$ phosphors for warm white light-emitting diodes, Opt. Mater. 89 (2019) 132–137, https://doi.org/10.1016/j.optmat.2019.01.012.
[14] X. Zhang, Z. Zhu, Z. Guo, Z. Sun, L. Zhou, Z. chao Wu, Synthesis, structure and luminescent properties of Eu^{3+} doped $Ca_3LiMgV_3O_{12}$ color-tunable phosphor, Ceram. Int. 44 (2018) 16514–16521, https://doi.org/10.1016/j.ceramint.2018.06.069.
[15] R. Cao, T. Chen, Y. Ren, C. Liao, Z. Luo, Y. Ye, Y. Guo, Tunable emission of $LiCa_3MgV_3O_{12}$:Bi^{3+} via energy transfer and changing excitation wavelength, Mater. Res. Bull. 111 (2019) 87–92, https://doi.org/10.1016/j.materresbull.2018.11.011.
[16] T. Hasegawa, Y. Abe, A. Koizumi, T. Ueda, K. Toda, M. Sato, Bluish-white luminescence in rare-earth-free vanadate garnet phosphors: structural characterization of $LiCa_3MV_3O_{12}$ (M = Zn and Mg), Inorg. Chem. 57 (2018) 857–866, https://doi.org/10.1021/acs.inorgchem.7b02820.
[17] H. Zhou, N. Guo, Q. Liang, Y. Ding, Y. Pan, Y. Song, R. Ouyang, Y. Miao, B. Shao, Novel ratiometric optical thermometry based on dual luminescent centers from europium doped $LiCa_3MgV_3O_{12}$ phosphor, Ceram. Int. 45 (2019) 16651–16657, https://doi.org/10.1016/j.ceramint.2019.05.207.
[18] X. Huang, H. Guo, $LiCa_3MgV_3O_{12}$:Sm^{3+}: a new high-efficiency white-emitting phosphor, Ceram. Int. 44 (2018) 10340–10344, https://doi.org/10.1016/j.ceramint.2018.03.043.
[19] A.A. Setlur, H.A. Comanzo, A.M. Srivastava, W.W. Beers, Spectroscopic evaluation of a white light phosphor for UV-LEDs—$Ca_2NaMgV_3O_{12}$:Eu^{3+}, J. Electrochem. Soc. 152 (2005) H205, https://doi.org/10.1149/1.2077328.
[20] G. Phosphor-in-glass, D. Pasinski, J. Sokolnicki, Damian Pasinski and Jerzy Sokolnicki, 2020. *.
[21] L. Yang, X. Mi, H. Zhang, X. Zhang, Z. Bai, J. Lin, Tunable luminescence and energy transfer properties in $Ca_2NaMg_2V_3O_{12}$: In^{3+} (Dy^{3+}, Sm^{3+}) phosphors, J. Alloys Compd. 787 (2019) 815–822, https://doi.org/10.1016/j.jallcom.2019.02.100.
[22] A.R. Dhobale, M. Mohapatra, V. Natarajan, S.V. Godbole, Synthesis and photoluminescence investigations of the white light emitting phosphor, vanadate garnet, $Ca_2NaMg_2V_3O_{12}$ co-doped with Dy and Sm, J. Lumin. 132 (2012) 293–298, https://doi.org/10.1016/j.jlumin.2011.09.004.
[23] X. Huang, S. Wang, S. Rtimi, B. Devakumar, $KCa_2Mg_2V3O_{12}$: a novel efficient rare-earth-free self-activated yellow-emitting phosphor, J. Photochem. Photobiol. Chem. 401 (2020), 112765, https://doi.org/10.1016/j.jphotochem.2020.112765.
[24] J. Li, K. Qiu, J. Li, W. Li, Q. Yang, J. Li, A novel broadband emission phosphor $Ca_2KMg_2V_3O_{12}$ for white light emitting diodes, Mater. Res. Bull. 45 (2010) 598–602, https://doi.org/10.1016/j.materresbull.2010.01.014.

[25] T. Jeyakumaran, N. Venkatesh Bharathi, R. Shanmugavel, P. Sriramachandran, S. Ramaswamy, Structural, vibrational, optical and improved photoluminescence properties of Dy^{3+} doped $Ca_2KZn_2V_3O_{12}$ phosphors, J. Inorg. Organomet. Polym. Mater. 31 (2021) 695–703, https://doi.org/10.1007/s10904-020-01766-5.

[26] Y. Li, X. Wei, H. Chen, G. Pang, Y. Pan, L. Gong, L. Zhu, G. Zhu, Y. Ji, A new self-activated vanadate phosphor of $Na_2YMg_2(VO_4)_3$ and luminescence properties in Eu^{3+} doped $Na_2YMg_2(VO_4)_3$, J. Lumin. 168 (2015) 124–129, https://doi.org/10.1016/j.jlumin.2015.08.002.

[27] Y. Tong, W.N. Zhang, R.F. Wei, L.P. Chen, H. Guo, $Na_2YMg_2(VO_4)_3$:Er^{3+},Yb^{3+} phosphors: up-conversion and optical thermometry, Ceram. Int. 47 (2021) 2600–2606, https://doi.org/10.1016/j.ceramint.2020.09.106.

[28] J. Zhou, X. Huang, J. You, B. Wang, H. Chen, Q. Wu, Synthesis, energy transfer and multicolor luminescent property of Eu^{3+}-doped $LiCa_2Mg_2V_3O_{12}$ phosphors for warm white light-emitting diodes, Ceram. Int. 45 (2019) 13832–13837, https://doi.org/10.1016/j.ceramint.2019.04.080.

[29] C. Manjunath, M.S. Rudresha, B.M. Walsh, R. Hari Krishna, B.S. Panigrahi, B. M. Nagabhushana, Optical absorption intensity analysis using Judd-Ofelt theory and photoluminescence investigation of orange-red Sr_2SiO_4: Sm^{3+}nanopigments, Dyes Pigments 148 (2018) 118–129, https://doi.org/10.1016/j.dyepig.2017.08.036.

[30] X. Huang, H. Guo, A novel highly efficient single-composition tunable white-light-emitting $LiCa_3MgV_3O_{12}$:Eu^{3+} phosphor, Dyes Pigments 154 (2018) 82–86, https://doi.org/10.1016/j.dyepig.2018.02.047.

[31] A. Bindhu, J.I. Naseemabeevi, S. Ganesanpotti, Vibrationally induced photophysical response of $Sr_2NaMg_2V_3O_{12}$:Eu^{3+} for dual-mode temperature sensing and safety signs, Adv. Photonics Res. 3 (2022), 2100159, https://doi.org/10.1002/adpr.202100159.

[32] S. Li, J. Guo, W. Shi, X. Hu, S. Chen, J. Luo, Y. Li, J. Kong, J. Che, H. Wang, B. Deng, R. Yu, Synthesis and characterization of wide band excited yellow phosphor $LaNb_2VO_9$:Dy^{3+} and application in potential fingerprint and lip print detection, J. Lumin. 244 (2022), 118681, https://doi.org/10.1016/j.jlumin.2021.118681.

[33] V. Vidyadharan, E. Sreeja, S.K. Jose, C. Joseph, N.V. Unnikrishnan, P.R. Biju, Spectroscopic and photoluminescence characterization of Dy^{3+} in $Sr_{0.5}Ca_{0.5}TiO_3$ phosphor, Luminescence 31 (2016) 202–209, https://doi.org/10.1002/bio.2946.

[34] L.S. Archana, D.N. Rajendran, An insight into the structure, luminescent characteristics and Judd-Ofelt analysis of (1-x) ZnS-(x) Dy_2O_3 phosphors, Mater. Sci. Semicond. Process. 128 (2021), 105752, https://doi.org/10.1016/j.mssp.2021.105752.

[35] T. Krishnapriya, A. Jose, T. Anna Jose, C. Joseph, N.V. Unnikrishnan, P.R. Biju, Luminescent kinetics of Dy^{3+} doped $CaZn_2(PO_4)_2$ phosphors for white light emitting applications, Adv. Powder Technol. 32 (2021) 1023–1032, https://doi.org/10.1016/j.apt.2021.02.003.

[36] V. Dimitrov, S. Sakka, Electronic oxide polarizability and optical basicity of simple oxides. I, J. Appl. Phys. 79 (1996) 1736–1740, https://doi.org/10.1063/1.360962.

[37] S. Tanabe, T. Ohyagi, N. Soga, T. Hanada, Compositional dependence of Judd-Ofelt parameters of Er^{3+} ions in alkali-metal borate glasses, Phys. Rev. B 46 (1992) 3305–3310, https://doi.org/10.1103/PhysRevB.46.3305.

[38] S. Tanabe, Rare-earth-doped glasses for fiber amplifiers in broadband telecommunication, Compt. Rendus Chem. 5 (2002) 815–824, https://doi.org/10.1016/S1631-0748(02)01449-2.

[39] I. Jlassi, H. Elhouichet, M. Ferid, C. Barthou, JuddOfelt analysis and improvement of thermal and optical properties of tellurite glasses by adding P_2O_5, J. Lumin. 130 (2010) 2394–2401, https://doi.org/10.1016/j.jlumin.2010.07.026.

[40] S.R. Yashodha, N. Dhananjaya, C. Manjunath, Synthesis and photoluminescence properties of Sm^{3+} doped LaOCl phosphor with reddish orange emission and it's Judd- Ofelt analysis, Mater. Res. Express 7 (2020), https://doi.org/10.1088/2053-1591/ab57a6.

[41] C. Manjunath, M.S. Rudresha, B.M. Walsh, R.H. Krishna, B.M. Nagabhushana, B. S. Panigrahi, Optical transition probabilities of white light emitting Sr_2SiO4:Dy^{3+} nanophosphors for lighting applications using Judd−Ofelt analysis, J. Lumin. 211 (2019) 437–445, https://doi.org/10.1016/j.jlumin.2019.03.054.

[42] R. Nagaraj, V. Rajagopal, A. Raja, S. Ranjith, Influence of Dy^{3+} ion concentration on photoluminescence and energy transfer mechanism of promising $KBaScSi_3O_9$ phosphors for warm white LEDs, Spectrochim. Acta Part A Mol. Biomol. Spectrosc. 264 (2022), 120212, https://doi.org/10.1016/j.saa.2021.120212.

[43] H. Lin, G. Meredith, S. Jiang, X. Peng, T. Luo, N. Peyghambarian, E. Yue-Bun Pun, Optical transitions and visible upconversion in Er^{3+} doped niobic tellurite glass, J. Appl. Phys. 93 (2003) 186–191, https://doi.org/10.1063/1.1527209.

[44] G.A. Kumar, E. De La Rosa, H. Desirena, Radiative and non radiative spectroscopic properties of Er^{3+} ion in tellurite glass, Opt Commun. 260 (2006) 601–606, https://doi.org/10.1016/j.optcom.2005.10.081.

[45] Y. Shi, J. Shi, C. Dong, Luminescence characteristics and J-O analysis of $BaWO_4$:3% Sm^{3+} crystal for yellow phosphors, Ceram. Int. 43 (2017) 16356–16361, https://doi.org/10.1016/j.ceramint.2017.09.009.

[46] J. An, S. Zhang, R. Liu, G. Hu, Z. Zhang, Y. Qiu, Y. Zhou, F. Zeng, Z. Su, Luminescent properties of Dy^{3+}/Eu^{3+} doped fluorescent glass for white LED based on oxyfluoride matrix, J. Rare Earths 39 (2021) 26–32, https://doi.org/10.1016/j.jre.2020.01.013.

[47] A. Ćirić, S. Stojadinović, M. Sekulić, M.D. Dramićanin, JOES: an application software for Judd-Ofelt analysis from Eu^{3+} emission spectra, J. Lumin. 205 (2019) 351–356, https://doi.org/10.1016/j.jlumin.2018.09.048.

[48] C. Dou, F. Zheng, S. Sun, R. Li, H. Xu, H. Kong, Y. Feng, S. Ullah, B. Teng, J. Tang, D. Zhong, Emission color tuning via modulating PO_4^{3-}/VO_4^{3-} proportion in Gd $(P_xV_{1-x})O_4$:1 at.% Dy^{3+}: a promising single-phased white-light-emitting phosphor, J. Lumin. 225 (2020), 117398, https://doi.org/10.1016/j.jlumin.2020.117398.

[49] L. Wang, L. Li, M. Yuan, Z. Yang, K. Han, H. Wang, X. Xu, Boltzmann- and non-Boltzmann-based thermometers in the first, second and third biological windows for the SrF_2:Yb^{3+}, Ho^{3+} nanocrystals under 980, 940 and 915 nm excitations, Nanoscale Res. Lett. 17 (2022), https://doi.org/10.1186/s11671-022-03718-z.

[50] P. Li, M. Jia, G. Liu, A. Zhang, Z. Sun, Z. Fu, Investigation on the fluorescence intensity ratio sensing thermometry based on nonthermally coupled levels, ACS Appl. Bio Mater. 2 (2019) 1732–1739, https://doi.org/10.1021/acsabm.9b00115.

[51] L. Lin, Z. Li, Z. Wang, Z. Feng, F. Huang, Q. Dai, Z. Zheng, Hypersensitive and color-tunable temperature sensing properties of (Eu,Tb)$(AcAc)_3$phen via phonon-assisted energy transfer, Opt. Mater. 110 (2020), 110532, https://doi.org/10.1016/j.optmat.2020.110532.

[52] A. Ćirić, S. Stojadinović, M.D. Dramićanin, An extension of the Judd-Ofelt theory to the field of lanthanide thermometry, J. Lumin. 216 (2019), 116749, https://doi.org/10.1016/j.jlumin.2019.116749.

[53] P. Du, Y. Hua, J.S. Yu, Energy transfer from VO_4^{3-} group to Sm^{3+} ions in $Ba_3(VO_4)_2$: 3xSm^{3+} microparticles: a bifunctional platform for simultaneous optical thermometer and safety sign, Chem. Eng. J. 352 (2018) 352–359, https://doi.org/10.1016/j.cej.2018.07.019.

[54] H. Guo, B. Devakumar, R. Vijayakumar, P. Du, X. Huang, A novel Sm^{3+} singly doped $LiCa_3ZnV_3O_{12}$ phosphor: a potential luminescent material for multifunctional applications, RSC Adv. 8 (2018) 33403–33413, https://doi.org/10.1039/c8ra07329e.

[55] Y. Luo, D. Zhang, S. Xu, L. Li, L. Chen, H. Guo, Optical thermometry based on Bi^{3+}, Ln^{3+} co-doped $YNbO_4$ (Ln = Dy, Eu) phosphors, J. Lumin. 257 (2023), 119780, https://doi.org/10.1016/j.jlumin.2023.119780.

[56] Q. Liu, M. Wu, B. Chen, X. Huang, M. Liu, Y. Liu, K. Su, X. Min, R. Mi, Z. Huang, Optical thermometry based on fluorescence intensity ratio of Dy^{3+}-Doped oxysilicate apatite warm white phosphor, Ceram. Int. 49 (2023), https://doi.org/10.1016/j.ceramint.2022.10.012.

[57] X. Yang, Q. Li, X. Li, B. Ma, Color tunable Dy^{3+}-doped $Sr_9Ga(PO_4)_7$ phosphors for optical thermometric sensing materials, Opt. Mater. 107 (2020), https://doi.org/10.1016/j.optmat.2020.110133.

[58] J. Zhang, L. Mei, Y. Zhang, Q. Guo, L. Liao, H. Liu, Influence of dysprosium concentration on sensitivity of luminescent thermometers of phosphors $Ca_9Tb(PO_4)_5(SiO_4)F_2$, J. Rare Earths 39 (2021) 946–951, https://doi.org/10.1016/j.jre.2020.08.013.

[59] J.Y. Li, D. Hou, Y. Zhang, H. Li, H. Lin, Z. Lin, W. Zhou, R. Huang, Luminescence, energy transfer and temperature sensing property of Ce^{3+}, Dy^{3+} doped $LiY_9(SiO_4)_6O_2$ phosphors, J. Lumin. 213 (2019) 184–190, https://doi.org/10.1016/j.jlumin.2019.05.027.